AIMS Mathematics, 11(3): 7436–7467.
DOI:10.3934/math.2026305
Received: 07 January 2026
Revised: 27 February 2026
Accepted: 16 March 2026
Published: 20 March 2026

https://www.aimspress.com/journal/Math

Research article

A novel one-parameter tri-modal alpha-skew logistic distribution: mathematical and reliability theory with applications to distant astronomical galaxies and biomedical data

Reda Elbarougy[1], Jondeep Das[2], Partha Jyoti Hazarika[3], G. G. Hamedani[4], Anupama Nandi[3] and Mohamed S. Eliwa[5,*]

[1] Department of Artificial Intelligence and Data Science, College of Computer Science and Engineering, University of Ha'il, Saudi Arabia
[2] Department of Statistics, Bhattadev University, Bajali, Assam, India
[3] Department of Statistics, Dibrugarh University, Dibrugarh, Assam, India
[4] Department of Mathematical and Statistical Sciences, Marquette University, USA
[5] Department of Statistics and Operations Research, College of Science, Qassim University, Saudi Arabia

* **Correspondence:** Email: m.eliwa@qu.edu.sa.

Abstract: In this paper, we presented a novel family of heavy-tailed continuous probability distributions tailored to model data exhibiting trimodal features with various kurtosis levels in asymmetric, under-dispersed datasets across various categories of risk. The proposed model enhanced the alpha-skew logistic distribution, providing significant adaptability to represent asymmetry and various tail characteristics. Key statistical properties were established, and additional characterizations were offered. Mathematical and numerical analyses indicated that the model efficiently handled asymmetric data, especially under conditions of under-dispersion. The associated hazard rate function displayed various forms, demonstrating the model's versatility in reliability and survival analysis. Parameter estimation was conducted using the maximum likelihood method, and simulation studies were employed to assess the performance of estimators in small samples. The practical applicability of the model was further demonstrated through analyses of two real datasets. Finally, comparative analyses with alternative models employing a likelihood ratio test substantiated its better performance.

Keywords: statistical model; multi-modality property; failure analysis; truncated moments; simulation; likelihood ratio test; data analysis
Mathematics Subject Classification: 60E05, 62E15, 62F10, 62N05, 62P99

1. Introduction

The innovative skew normal distribution presented in [4] serves as a natural extension of the normal distribution with the inclusion of an additional asymmetry parameter. The probability density function (PDF) of the skew normal distribution is given by

$$f(x;\lambda) = 2\,\phi(x)\,\Phi(\lambda x), \qquad x \in \mathbb{R},\ \lambda \in \mathbb{R}, \tag{1.1}$$

where $\phi(\cdot)$ and $\Phi(\cdot)$ denote the PDF and the cumulative distribution function (CDF) of the standard normal distribution, respectively. With the research in [4] being a pioneering discovery, a wide scope of research emerged on skewed distributions. These research works led to several new derivations by introducing asymmetric versions of well-known symmetric distributions, offering greater flexibility and broader applicability. For example, the researchers in [24] introduced the skew logistic distribution by using the PDF and CDF of the logistic distribution in place of the standard normal PDF and CDF models in [4]. Similarly, the researchers in [3] proposed the skew Laplace distribution as an asymmetric extension of the Laplace distribution.

The logistic distribution, which is frequently viewed as a rival to the normal and Laplace distributions, is an important distribution that has drawn significant interest from theoretical and application points of view [18]. For this reason, a continuous study on the skewed version of the logistic distribution from different perspectives has been carried out for many decades. Some notable contributions towards this approach were reflected in the research works done by [22] etc. Until then, a few studies were carried out on the topic of skewed distribution, supporting bimodality as well as tri-modality of the data. The presence of bimodality for some cancers was detected by the researchers in [1]. Following the presence of bimodality, some studies are found in the literature with the presence of tri-modality behavior of the data. For example, to deal with the problems of attitudinal polarization, tri-modality was proposed in [8] as a distributional pattern to the conceptual issues of polarization. They demonstrated that attitudes were present toward a central tendency and distinct tails in Likert-type measures featuring a midway. Conversely, the researchers in [13] revealed the presence of tri-modality in the distribution of relative earnings during the examination of the growth of West German regions. The analysis of the classification of 71 West German regions into three distinct income clubs indicated that the distribution of relative incomes became tri-modal. Moreover, the researchers in [5] and [37] showed that trauma fatalities in urban settings in the US have a tri-modal distribution. They demonstrated that plotting the death rate for a substantial sample of fatalities as a function of time post-injury revealed a tri-modal distribution. They categorized the initial peak as "Immediate deaths", signifying that persons die instantly; the subsequent peak as "Early deaths", indicating that individuals die within the first few hours; and the third peak as "Late deaths," denoting that individuals die days or weeks post-injury. A tri-modal distribution for the lengths of the metal-oxygen bridging bonds in Keggin molybdates was also shown in [40]. A histogram showing all metal-oxygen bridging bonds was made for the Lindqvist (a), Keggin (b), and Dawson (c) cluster types. Each one had a tri-modal distribution. The grey bars show M-O-W bonds, whereas the white bars show M-O-Mo bonds. Moreover, the researchers in [23] established that the grid indentation data necessitated a tri-modal fit. The researchers encountered challenges in executing the statistical analysis of the grid indentation data while delineating two methodologies for instrumented indentation to assess the mechanical properties of thermal spray coatings (TSC). A tri-modal Gaussian distribution was required to encapsulate the

attributes of particular phases, and the subsequently extracted features were successfully incorporated into the study.

Thus, in a practical scenario, great importance lies in the development of bimodal and tri-modal skew distributions. Some researchers have led to the development of new families of symmetric as well as asymmetric distributions that enable the data to match up to two and three modes. For example, by extending the skew-normal model of [4], the researchers in [19] proposed a class of two-piece skew-normal distribution involving linear and non-linear constraints, which is a skewed extension of the extended two-piece normal distribution discussed by the researchers in [2]. Alpha skew normal (ASN) distribution was another new family of distribution introduced by the researchers in [10] which is flexible enough to fit data up to two modes. With the same concept, the researchers in [17] proposed the alpha skew logistic distribution (ASLG), generalizing logistic distribution to uni-modal and bimodal datasets. The PDF of the ASLG model can be provided as

$$f(x;\alpha) = \left(\frac{3(1-\alpha)^2+1}{6+\alpha^2\pi^2}\right)\left(\frac{e^{-x}}{(1+e^{-x})^2}\right), \qquad x \in \mathbb{R},\ \alpha \in \mathbb{R}, \tag{1.2}$$

where $x \in \mathbb{R}$ and $\alpha > 0$. Beyond these developments, the literature has documented several other families of skewed distributions capable of accommodating bimodal data. Notable examples included the generalized alpha skew normal distribution [36], the Balakrishnan alpha skew logistic distribution [31], the Log-Balakrishnan alpha skew normal distribution [32], and the Balakrishnan alpha skew generalized t distribution [27]. The researchers in [30] introduced a novel family of skew distributions, namely the alpha beta skew normal (ABSN) distribution, which demonstrated sufficient flexibility to accommodate data with up to four modes. Building on this concept, the researchers in [12] proposed the alpha-beta skew logistic family. Subsequently, the researchers in [34] developed a generalized alpha-beta skew normal distribution that offered enhanced flexibility compared to the ABSN distribution in [30]. Additional families of skew distributions supporting data with up to four modes included the Balakrishnan alpha-beta skew normal distribution [33] and the Balakrishnan alpha beta skew Laplace distribution [35]. Furthermore, for modeling multimodal data, the researchers in [21] constructed several new flexible classes of normal distributions. For more discussions of various forms of skewed models, readers may consult [11,20,39]. Tri-modal normal (TN) distribution was one symmetric distribution introduced throughout this study, whose PDF is defined as

$$f(x) = \left(\frac{(x^2-1)^2}{4}\right)\left(\frac{e^{-x}}{(1+e^{-x})^2}\right), \qquad x \in \mathbb{R}. \tag{1.3}$$

Borrowing the same concept, tri-modal logistic (TLG) distribution was introduced by the researchers in [26] with the PDF

$$f(x) = \left(\frac{(x^2-1)^2}{C_1}\right)\left(\frac{e^{-x}}{(1+e^{-x})^2}\right), \qquad x \in \mathbb{R}, \tag{1.4}$$

where $C_1 = \frac{1}{15}\left(45 - 10\pi^2 + 3\pi^4\right)$. Later, some other distributions, namely flexible alpha skew normal distribution [7] and flexible alpha skew logistic distribution [9], were introduced as some generalizations of those in [21]. Moreover, multimodal distributions have attracted increasing attention due to their strong applicability in modeling complex real-world data arising in environmental, biomedical, and reliability studies. For instance, the researchers in [25] investigated a bimodal

Gumbel-type model and demonstrated its effectiveness in analyzing environmental datasets exhibiting heterogeneous extreme-value behavior. Similarly, developments in flexible multimodal distributional frameworks have been shown to provide improved goodness-of-fit and interpretability in applied statistical modeling (see, e.g., [38]). These studies highlight the growing importance of multimodal models in contemporary applied literature and further motivate the development of the proposed tri-modal alpha-skew logistic distribution.

Although many classical reliability datasets exhibit over-dispersion due to heterogeneous populations, latent competing risks, or environmental variability, under-dispersion also arises in several practical contexts. For example, highly standardized manufacturing processes with strict quality control may produce tightly clustered component lifetimes. Similarly, in complex systems with overlapped failure mechanisms, the effective aggregation of dependent subcomponent risks may reduce variability in observed system-level failure times. Controlled biomedical survival studies involving homogeneous cohorts may likewise demonstrate reduced dispersion. In such settings, models capable of accommodating lighter variability while preserving flexible modality structures are essential. The TASL distribution provides this adaptability through the shape parameter α, which simultaneously regulates dispersion, skewness, and modality. In particular, moderate to large positive values of α yield reduced variance and sharper central concentration, making the model suitable for under-dispersed reliability data while enabling heavier-tailed or multimodal configurations when required.

In this article, a new extension of the alpha skew logistic distribution in [17] is proposed, considering the polynomial of tri-modal logistic distribution. Additionally, the flexibility and usefulness of the proposed model is checked with the help of real-life applications. A simulation study is also performed to check the effectiveness of the estimates of the parameter of the newly induced distribution. Compared to finite mixtures of logistic distributions, the proposed model offers a more interpretable framework for modeling multimodal data. While a three-component logistic mixture requires multiple mixing proportions and component-specific parameters, the proposed construction achieves trimodality through a single shape parameter. This significantly enhances parameter interpretability, as the same parameter simultaneously governs skewness, tail behavior, and modality. Moreover, the absence of latent mixture components avoids common computational challenges such as identifiability issues, label switching, and convergence instability in likelihood-based estimation. As a result, the proposed model provides a computationally efficient and statistically stable alternative to finite mixture approaches, particularly for moderate sample sizes. While strictly tri-modal failure time distributions may be uncommon in classical mechanical and electronic component reliability, multimodal lifetime behavior can arise in heterogeneous populations, repairable systems, biomedical survival studies, and systems experiencing distinct early-life, random, and wear-out phases. The proposed model therefore serves as a flexible general framework capable of accommodating unimodal, bimodal, or trimodal structures within a unified parametric setting rather than being restricted to exclusively tri-modal engineering applications.

The remainder of this article was organized as follows: In Section 2, a new extension of the alpha skew logistic distribution was derived along with its graphical visualizations and some special cases. In Section 3, important statistical properties of the new distribution were discussed, while the results of the characterization of the same distribution were included in Section 4. Section 5 was devoted to the estimation of the parameter of the induced distribution. In Section 6, the results of the simulation studies were presented. Section 7 examined real-life applications of the proposed distribution to assess

its flexibility. Section 8 performed likelihood ratio tests to discriminate between the proposed model and other nested models, while Section 9 concluded the article.

2. A new family of logistic distribution: mathematical theory and visualization

Let X be a continuous random variable. Then X is said to follow the tri-modal alpha skew logistic (TASL) distribution if its PDF is given by

$$f(x;\alpha) = \frac{1}{C(\alpha)}\Big((1-\alpha x)^2+1\Big)\Big(\big(x^2-1\big)^2+2\Big)\left(\frac{e^{-x}}{(e^{-x}+1)^2}\right), \tag{2.1}$$

where α is the shape parameter and $C(\alpha)$ is the normalizing constant, given by

$$C(\alpha) = \frac{1}{105}\left(155\pi^6\alpha^2 - 98\pi^4(\alpha^2-1) + 35\pi^2(3\alpha^2-4) + 630\right).$$

The TASL distribution can exhibit at most three modes. By differentiating the PDF as given in Eq (2.1), we obtain

$$\begin{aligned} f'(x;\alpha,\lambda) = -\frac{1}{C(\alpha)}\Bigg[105e^x\Bigg(&6(\alpha-1) - \alpha^2x^6 + 2\alpha(1-3\alpha)x^5 + 2(\alpha^2+5\alpha-1)x^4 \\ &+ (8\alpha^2-4\alpha-8)x^3 + (-3\alpha^2-12\alpha+4)x^2 + e^x\Big(6(\alpha+1) + \alpha^2x^6 \\ &- 2\alpha(3\alpha+1)x^5 - 2(\alpha^2-5\alpha-1)x^4 + 4(2\alpha^2+\alpha-2)x^3 + (3\alpha^2-12\alpha-4)x^2 \\ &+ (-6\alpha^2-6\alpha+8)x\Big) + (-6\alpha^2+6\alpha+8)x\Bigg)\Bigg]. \end{aligned} \tag{2.2}$$

Setting $f'(x;\alpha,\lambda) = 0$, we get

$$\begin{aligned} 105e^x\Bigg(&6(\alpha-1) - \alpha^2x^6 + 2\alpha(1-3\alpha)x^5 + 2(\alpha^2+5\alpha-1)x^4 \\ &+ (8\alpha^2-4\alpha-8)x^3 + (-3\alpha^2-12\alpha+4)x^2 + e^x\Big(6(\alpha+1) + \alpha^2x^6 \\ &- 2\alpha(3\alpha+1)x^5 - 2(\alpha^2-5\alpha-1)x^4 + 4(2\alpha^2+\alpha-2)x^3 + (3\alpha^2-12\alpha-4)x^2 \\ &+ (-6\alpha^2-6\alpha+8)x\Big) + (-6\alpha^2+6\alpha+8)x\Bigg) = 0. \end{aligned} \tag{2.3}$$

Thus, $f'(x;\alpha)$ has at most five zeros, and the PDF $f(x;\alpha)$ can have at most three modes. Although the proposed PDF can exhibit at most three modes, the occurrence of exactly three modes depends on the number and nature of the real solutions of the first derivative. In particular, tri-modality arises only when the score equation admits three distinct real critical points that satisfy the second-derivative conditions for local maxima. Moreover, imposing additional constraints such as equal peak heights (equal-depth modes) or equal curvature/width at the modes leads to a system of highly nonlinear equations involving polynomial and exponential terms. Owing to this analytical complexity, such conditions do not yield closed-form solutions and must be examined numerically for specific parameter values. Consequently, equal-depth or equal-width tri-modal configurations are characterized through numerical exploration rather than explicit analytical expressions.

Some special cases of the TASL distribution are given below:

(1) For $\alpha = 0$, the PDF of the TASL distribution reduces to a symmetric form, given by

$$f(x) = \frac{210\, e^{-x}\left[(x^2-1)^2+2\right]}{(630 - 140\pi^2 + 98\pi^4)\,(1+e^{-x})^2}. \tag{2.4}$$

This reduced form may be referred to as the trimodal alpha logistic (TAL) distribution.

(2) If $X \sim \text{TASL}(\alpha)$, then $-X \sim \text{TASL}(-\alpha)$.

The plots in Figure 1 illustrate the behavior of the PDF of the TASL distribution under various choices of shape parameter α. Panels (a)–(d) display how changes in α influence modality, tail behavior, and peak sharpness. Parameter α plays a central and multifaceted role in the proposed TASL distribution. It also governs the degree and direction of skewness, tail heaviness, overall dispersion, and the modality structure of the distribution. Small values of α typically produce heavier tails and stronger asymmetry, whereas larger values of α lead to lighter tails, reduced dispersion, and increasingly symmetric shapes. Moreover, variations in α directly affect the number, location, and relative prominence of the modes, enabling the distribution to transition smoothly between unimodal, bimodal, and trimodal configurations. Hence, the parameter α serves as the primary flexibility parameter of the model, enabling it to accommodate a wide range of distributional behaviors observed in practice.

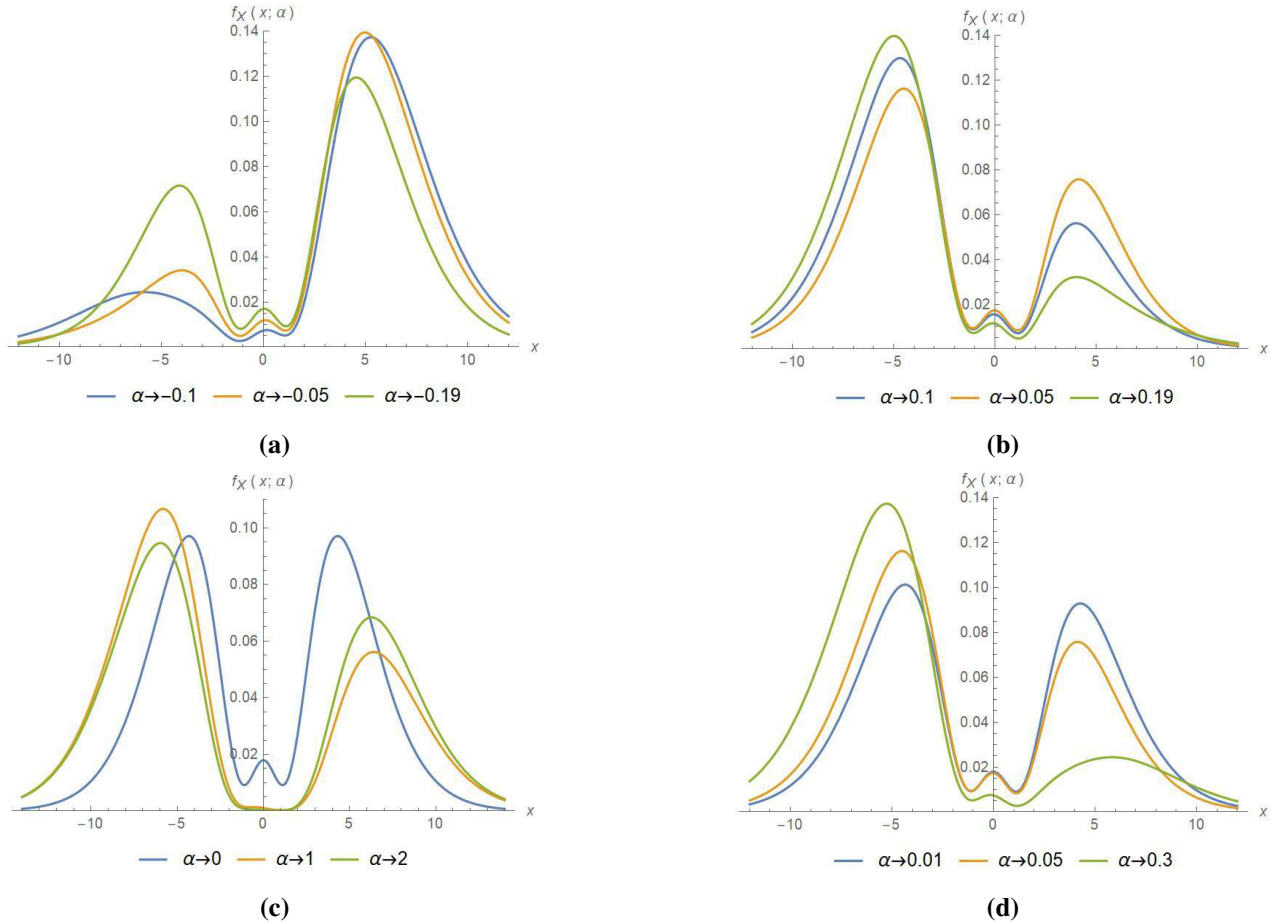

Figure 1. The PDF plots of TASL distribution for different parameter values.

In panels (a) and (b), for small negative values of α, the distribution exhibits noticeable asymmetry with a clear bimodal structure. As α increases from -0.19 to -0.05 and -0.01, the leftmost mode becomes more pronounced, while the right tail becomes slightly lighter, indicating a shift in mass toward the center. Panel (c) demonstrates the effect of taking α as a positive parameter. For $\alpha = 0, 1$, and 2, the bimodality becomes more prominent with sharper peaks, and the right mode shifts rightward with increasing α. This behavior highlights the flexibility of the TASL distribution in modeling highly heterogeneous data. Panel (d) presents moderate positive values ($\alpha = 0.01, 0.05, 0.3$). Furthermore, increasing the α concentration around the component modes reduces the dispersion between them, showing the distribution's ability to adjust peak heights while maintaining overall shape characteristics. Using the PDF presented in (2.1), the CDF is defined as

$$\begin{aligned} F(x;\alpha) = P(X \le x) &= \frac{1}{C(\alpha)} \int_{-\infty}^{x} [(1-\alpha x)^2 + 1][(x^2-1)^2 + 2] \frac{e^{-x}}{(1+e^{-x})^2}\, dx \\ &= \frac{1}{C(\alpha)} \Big[\alpha^2 I_1 - 2\alpha I_2 + (2-2\alpha^2) I_3 + 4\alpha I_4 + (3\alpha^2 - 4) I_5 - 6\alpha I_6 + 6 I_7\Big]. \end{aligned}$$

It can be observed that the integrals I_5, I_6, and I_7 coincide with those appearing in the CDF of the alpha skew logistic distribution and I_7 coincides with those appearing in the CDF of the alpha skew logistic distribution [17], and the corresponding results are employed directly in this derivation. The remaining integrals are evaluated using integration by parts. Moreover, substituting the resulting expressions and simplifying, the CDF of the TASL distribution is obtained as

$$\begin{aligned} F(x;\alpha) = \frac{1}{C(\alpha)} \Bigg[&\frac{e^x}{1+e^x} P_1(x) + 2\log(1+e^x) P_2(x) + P_3(x) \operatorname{Li}_2(-e^x) + 24 P_4(x) \operatorname{Li}_3(-e^x) \\ &- 24 P_5(x) \operatorname{Li}_4(-e^x) + 10\alpha \Big\{(1-3x\alpha) \operatorname{Li}_5(-e^x) + 3\alpha \operatorname{Li}_6(-e^x)\Big\}\Bigg], \end{aligned} \tag{2.5}$$

where $\operatorname{Li}_n(x) = \sum_{k=1}^{\infty} x^k/k^n$ denotes the polylogarithm function [28]. The polynomials appearing above are given by

$$\begin{aligned} P_1(x) &= (x^4 - 2x^2 + 3)(2 + x\alpha(x\alpha - 2)), \\ P_2(x) &= 3\alpha + (4 - 4x^2 + x(5x^2 - 6))\alpha - (3x^4 - 4x^2 + 3)\alpha^2, \\ P_3(x) &= 3\alpha + x(4 - 4x^2 + \alpha(5x^2 - 6)) - (3x^4 - 4x^2 + 3)\alpha^2, \\ P_4(x) &= \alpha + x(2 + \alpha(2\alpha + 5x(x\alpha - 1))), \\ P_5(x) &= 2 + \alpha(2 - \alpha + 5x(3x\alpha - 2)). \end{aligned}$$

Figure 2 displays the CDF of the TASL distribution for several values of parameter α. Panels (a) and (b) show how the shape of the CDF responds to positive and negative values of α. In panel (a), when α varies across $-0.6, 0, 0.6$, and 4.5, the steepness of the CDF changes significantly. Larger positive values of α yield a steeper rise in the central region, indicating reduced spread and faster accumulation of probability mass. Conversely, negative values of α produce a more gradual increase, corresponding to heavier tails and greater dispersion. Panel (b) explores moderate values ($\alpha = -0.35, 0.43, 0.8$, and -0.8). Negative α again corresponds to heavier left tails, delaying the rise of the CDF, whereas positive α accelerates the transition from 0 to 1. As α becomes larger, the CDF transitions become more concentrated around the central region, signifying reduced variability.

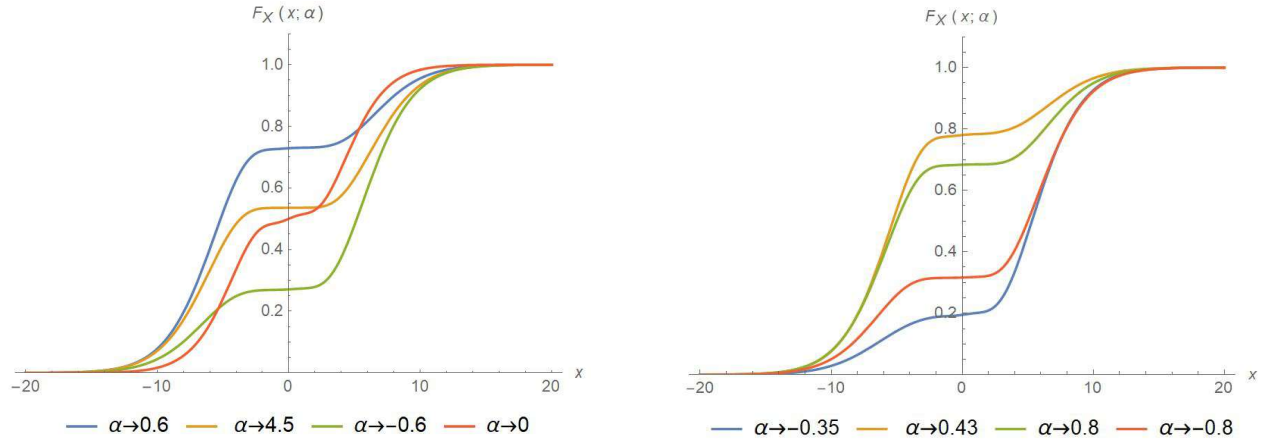

(a) **(b)**

Figure 2. The CDF plots of TASL distribution for different parameter values.

3. Statistical properties

3.1. Moment-based measures and related properties

To derive the r^{th} moments of the TASL model, we utilize the r^{th} moments of the standard logistic distribution (see, [14]). If $Z \sim L(0, 1)$, i.e., Z follows the standard logistic distribution, then its moments are given by

$$E(Z^r) = \begin{cases} 2\left(1 - \frac{1}{2^{r-1}}\right)\Gamma(r+1)\zeta(r), & \text{for even } r, \\ 0, & \text{for odd } r, \end{cases} \tag{3.1}$$

where $\zeta(s) = \sum_{j=1}^{\infty} j^{-s}$ is the Riemann Zeta function and $\Gamma(s) = \int_0^{\infty} t^{s-1}e^{-t}dt$ is the Gamma function. From the PDF in (2.1), the r^{th} moment of X is

$$\begin{aligned} E(X^r) &= \frac{1}{C(\alpha)} \int_{-\infty}^{\infty} x^r[(1-\alpha x)^2 + 1][(x^2-1)^2 + 2]\frac{e^{-x}}{(1+e^{-x})^2}\,dx \\ &= \frac{1}{C(\alpha)}\Bigg[\alpha^2 \int_{-\infty}^{\infty} x^{r+6}\frac{e^{-x}}{(1+e^{-x})^2}dx - 2\alpha \int_{-\infty}^{\infty} x^{r+5}\frac{e^{-x}}{(1+e^{-x})^2}dx \\ &\quad + (2-2\alpha^2)\int_{-\infty}^{\infty} x^{r+4}\frac{e^{-x}}{(1+e^{-x})^2}dx + 4\alpha \int_{-\infty}^{\infty} x^{r+3}\frac{e^{-x}}{(1+e^{-x})^2}dx \\ &\quad + (3\alpha^2-4)\int_{-\infty}^{\infty} x^{r+2}\frac{e^{-x}}{(1+e^{-x})^2}dx - 6\alpha \int_{-\infty}^{\infty} x^{r+1}\frac{e^{-x}}{(1+e^{-x})^2}dx + 6\int_{-\infty}^{\infty} x^r\frac{e^{-x}}{(1+e^{-x})^2}dx\Bigg]. \end{aligned} \tag{3.2}$$

Using (3.1), the even r^{th}-order moment simplifies to

$$\begin{aligned} E(X^{2r}) = \frac{2}{C(\alpha)}\Bigg[&\alpha^2\left(1 - \frac{1}{2^{r+5}}\right)\Gamma(r+7)\zeta(r+6) + (2-2\alpha^2)\left(1 - \frac{1}{2^{r+3}}\right)\Gamma(r+5)\zeta(r+4) \\ &+ (3\alpha^2-4)\left(1 - \frac{1}{2^{r+1}}\right)\Gamma(r+3)\zeta(r+2) + 6\left(1 - \frac{1}{2^{r-1}}\right)\Gamma(r+1)\zeta(r)\Bigg]. \end{aligned} \tag{3.3}$$

Similarly, for the even r^{th}-order moment, we obtain

$$E(X^{2r-1}) = \frac{2}{C(\alpha)}\Bigg[-2\alpha\left(1-\frac{1}{2^{r+4}}\right)\Gamma(r+6)\zeta(r+5)+4\alpha\left(1-\frac{1}{2^{r+2}}\right)\Gamma(r+4)\zeta(r+3) - 6\alpha\left(1-\frac{1}{2^{r}}\right)\Gamma(r+2)\zeta(r+1)\Bigg]. \tag{3.4}$$

It is worth noting that although the Riemann zeta function has a pole at unity, the moment expressions of the proposed distribution involve $\zeta(r+k)$ with $k \geq 2$, ensuring that the arguments always exceed one. Hence, all moments of finite order exist. Now, using (3.3) and (3.4) with $r = 1, 2, 3, 4$, the first four raw moments are

$$E(X) = \frac{-2\pi^2\alpha\left(105-98\pi^2+155\pi^4\right)}{105C(\alpha)},$$

$$E(X^2) = \frac{\pi^2\left(889\pi^6\alpha^2-310\pi^4(\alpha^2-1)+49\pi^2(3\alpha^2-4)+210\right)}{105C(\alpha)},$$

$$E(X^3) = \frac{-2\pi^4\alpha\left(147-310\pi^2+889\pi^4\right)}{105C(\alpha)},$$

$$E(X^4) = \frac{\pi^4}{C(\alpha)}\left[\frac{2555\pi^6\alpha^2}{33}-\frac{254}{15}\pi^4(\alpha^2-1)+\frac{31}{21}\pi^2(3\alpha^2-4)+\frac{14}{5}\right].$$

Hence, the variance of the TASL distribution is

$$\mathrm{Var}(X) = \frac{1}{[105C(\alpha)]^2}\Bigg[\pi^2\Big\{-4\pi^2\alpha^2(105-98\pi^2+155\pi^4)+105C(\alpha)\Big(210+889\pi^6\alpha^2 - 310\pi^4(\alpha^2-1)+49\pi^2(3\alpha^2-4)\Big)\Big\}\Bigg].$$

By optimizing $E(X)$ and $\mathrm{Var}(X)$ with respect to α, the bounds for the mean and variance are derived as

$$-3.98 \leq E(X) \leq 3.98, \qquad 26.35 \leq \mathrm{Var}(X) \leq 58.02.$$

Figure 3(a) and (b) show these limits graphically as well.

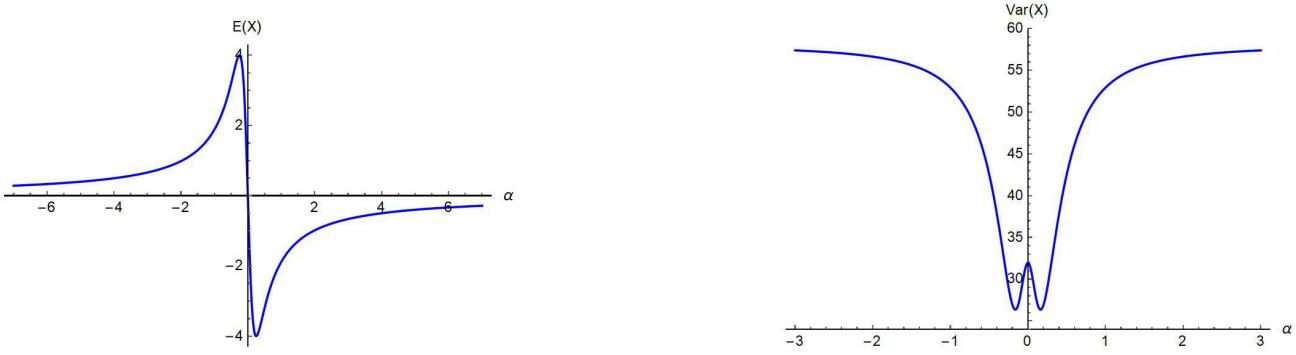

(a) **(b)**

Figure 3. Plots of mean and variance of TASL distribution for different parameter choices.

The expression of mean, variance, skewness, and kurtosis coefficient of TASL distribution contains very complex mathematical forms, and hence, some numerical values of the above statistical measures for the TASL distribution are listed in Table 1 for different values of the parameter.

Table 1. Mean, variance, skewness, and kurtosis of the distribution for selected values of α.

α	Mean (μ)	Variance (σ^2)	Skewness (γ_1)	Kurtosis (γ_2)
-2.0	3.625	0.603	0.492	3.40
-1.0	2.837	0.986	0.743	3.97
-0.5	2.253	1.478	1.116	4.87
0.5	2.253	1.478	1.116	4.87
1.0	2.837	0.986	0.743	3.97
2.0	3.625	0.603	0.492	3.40
3.0	4.128	0.470	0.392	3.23
5.0	4.786	0.373	0.310	3.12

From Table 1, it can be observed that the mean of the distribution increases monotonically with $|\alpha|$. Larger values of $|\alpha|$ shift the mass of the distribution toward the right, leading to a steady increase in the expected value. Again, the variance decreases as $|\alpha|$ increases, indicating that the distribution becomes more concentrated around its mean. For moderate to large $|\alpha|$, the variance becomes substantially smaller, demonstrating a sharper and more peaked structure. Besides, the coefficient of skewness γ_1 is positive for all values of α, implying a right-skewed distribution. The skewness decreases as $|\alpha|$ increases, showing that the distribution becomes more symmetric. For small $|\alpha|$ (e.g., $\alpha = \pm 0.5$), the skewness is relatively high, while for larger magnitudes (e.g., $\alpha = \pm 3$ or ± 5), the skewness approaches values close to zero. The kurtosis γ_2 decreases toward the value 3, which corresponds to the kurtosis of the normal distribution. For small $|\alpha|$, the distribution exhibits heavy tails (kurtosis > 4), whereas for larger $|\alpha|$, the tails become lighter and the distribution approaches a mesokurtic shape. Hence, parameter α primarily controls the tail weight and asymmetry of the distribution. Small $|\alpha|$ produces a heavy-tailed and highly right-skewed shape, whereas large $|\alpha|$ yields a distribution that is nearly symmetric and close to normal in terms of both kurtosis and dispersion.

3.2. Moment generating function and corresponding cumulants

Using the PDF of the TASL distribution given in (2.1), the moment generating function (MGF) is defined as

$$
\begin{aligned}
M(t) = \mathbb{E}[e^{tX}] &= \int_{-\infty}^{\infty} e^{tx} f(x;\alpha)\,dx = \frac{1}{C(\alpha)} \int_{-\infty}^{\infty} e^{tx}[(1-\alpha x)^2 + 1][(x^2-1)^2 + 2] \frac{e^{-x}}{(1+e^{-x})^2}\,dx \\
&= \frac{1}{C(\alpha)}\Bigg[\alpha^2 \int_{-\infty}^{\infty} x^6 e^{tx} \frac{e^{-x}}{(1+e^{-x})^2}\,dx - 2\alpha \int_{-\infty}^{\infty} x^5 e^{tx} \frac{e^{-x}}{(1+e^{-x})^2}\,dx \\
&\quad + (2-2\alpha^2) \int_{-\infty}^{\infty} x^4 e^{tx} \frac{e^{-x}}{(1+e^{-x})^2}\,dx + 4\alpha \int_{-\infty}^{\infty} x^3 e^{tx} \frac{e^{-x}}{(1+e^{-x})^2}\,dx \\
&\quad + (3\alpha^2 - 4) \int_{-\infty}^{\infty} x^2 e^{tx} \frac{e^{-x}}{(1+e^{-x})^2}\,dx - 6\alpha \int_{-\infty}^{\infty} x e^{tx} \frac{e^{-x}}{(1+e^{-x})^2}\,dx + 6 \int_{-\infty}^{\infty} e^{tx} \frac{e^{-x}}{(1+e^{-x})^2}\,dx\Bigg]
\end{aligned}
$$

$$= \frac{1}{C(\alpha)}[\alpha^2 I_8 - 2\alpha I_9 + (2 - 2\alpha^2)I_{10} + 4\alpha I_{11} + (3\alpha^2 - 4)I_{12} - 6\alpha I_{13} + 6I_{14}]. \tag{3.5}$$

Here, the auxiliary polynomials are defined as

$$\begin{aligned}
P_6(x) &= (\pi^4 + 2\pi^2 + 3)(\pi^2\alpha^2 - 2),\\
P_7(x) &= 4 + \pi^4\alpha(t - 3\alpha) + 3\alpha(t - \alpha) + 2\pi^2(2 + (t - 2\alpha)\alpha),\\
P_8(x) &= (-4t(5\pi^2 + 1) + 4\alpha(25\pi^2 + 3)) + (91\pi^4 + 20\pi^2 + 3),\\
P_9(x) &= 2 + \alpha(t + 5\pi^2 t - (15\pi^2 + 2)),\\
P_{10}(x) &= (10\alpha + t(\alpha^2(35\pi^2 + 2) - 2)) + 10\pi\alpha(3\alpha - t)\cot(\pi t).
\end{aligned}$$

It can be observed that I_{12}, I_{13}, and I_{14} are the same functions involved in the MGF of the alpha skew logistic distribution [17], and their results are used in this derivation. The remaining integrals are computed using integration by parts. After simplification, the MGF of the TASL distribution is obtained as

$$\begin{aligned}
M(t) = \frac{\pi\csc(\pi t)}{4C(\alpha)}\Big[&- 8\alpha(5\pi^4 + 6\pi^2 + 3) - 4tP_6(x) + 8\pi P_7(x)\cot(\pi t) + t\alpha^2\pi P_8(x)\\
&- 12\pi P_9(x)\alpha\cot(\pi t)\csc^2(\pi t) - 12\pi^3 P_{10}(x)\cot(\pi t)\csc^4(\pi t) + 360\pi^5 + \alpha^2\csc^6(\pi t)\Big].
\end{aligned}$$

Hence, the characteristic function is obtained as

$$\begin{aligned}
\phi(t) = \frac{\pi\csc(\pi it)}{4\,C(\alpha)}\Big[&- 8\alpha(5\pi^4 + 6\pi^2 + 3) - 4t\,P_6(x) + 8\pi\,P_7(x)\cot(\pi it) + it\,\alpha^2\pi\,P_8(x)\\
&- 12\pi\,P_9(x)\,\alpha\cot(\pi it)\csc^2(\pi it) - 12\pi^3 P_{10}(x)\cot(\pi it)\csc^4(\pi it) + 360\pi^5 + \alpha^2\csc^6(\pi it)\Big].
\end{aligned}$$

Taking the natural logarithm of the MGF, the cumulant generating function (CGF) of the TASL distribution is obtained as

$$\begin{aligned}
K(t) = \log\left(\frac{\pi}{4\,C(\alpha)}\right) - \log(\sin(\pi t)) + \log\Big[&- 8\alpha(5\pi^4 + 6\pi^2 + 3) - 4t\,P_6(x) + 8\pi\,P_7(x)\cot(\pi t)\\
&+ t\alpha^2\pi P_8(x) - 12\pi\,P_9(x)\alpha\cot(\pi t)\csc^2(\pi t) - 12\pi^3 P_{10}(x)\cot(\pi t)\csc^4(\pi t) + 360\pi^5 + \alpha^2\csc^6(\pi t)\Big].
\end{aligned}$$

3.3. Average absolute deviation

The extent of dispersion within a population can be partially assessed using the total deviation from both the mean and the median. These quantities, known as the mean deviation about the mean and the mean deviation about the median, are defined by

$$\delta_1(X) = \int_{-\infty}^{\infty} |x - \mu| f(x)\,dx, \qquad \delta_2(X) = \int_{-\infty}^{\infty} |x - M| f(x)\,dx,$$

where $\mu = E(X)$ and M denotes the median. Thus, $\delta_1(X)$ can be written as

$$\delta_1(X) = \int_{-\infty}^{\infty} |x - \mu| f(x)\,dx = 2\mu F(\mu) - 2\int_{-\infty}^{\mu} x f(x)\,dx = 2\mu F(\mu) - 2I_9(x),$$

where $\mu = E(X)$ is obtained from Eq (3.4). Now, $I_9(x)$ is derived as

$$I_9(x) = \int_{-\infty}^{\mu} x\, f(x;\alpha)\, dx = \frac{1}{C(\alpha)} \int_{-\infty}^{\mu} \left[(1-\alpha x)^2 + 1\right]\left[(x^2-1)^2 + 2\right] \frac{e^{-x}}{(1+e^{-x})^2}\, dx.$$

The integral contains a highly complex structure, and after simplification, its final closed-form expression becomes

$$I_9(x) = \frac{1}{C(\alpha)}\Bigg[\frac{e^{\mu}}{1+e^{\mu}} A(\mu,\alpha) + B(\mu,\alpha)\, \log(1+e^{\mu}) - 2P_1(\mu,\alpha)\, \mathrm{Li}_2(-e^{\mu}) + 6P_2(\mu,\alpha)\, \mathrm{Li}_3(-e^{\mu}) + C_4(\mu,\alpha)\, \mathrm{Li}_4(-e^{\mu}) + C_5(\mu,\alpha)\, \mathrm{Li}_5(-e^{\mu}) + C_6(\mu,\alpha)\, \mathrm{Li}_6(-e^{\mu}) + C_7(\mu,\alpha)\, \mathrm{Li}_7(-e^{\mu})\Bigg].$$

Substituting this into the previous expression, the final form of the mean deviation about the mean is obtained as

$$\delta_1(X) = 2\mu F(\mu) - \frac{2}{C(\alpha)}\Bigg[\frac{e^{\mu}}{1+e^{\mu}} A(\mu,\alpha) + B(\mu,\alpha)\, \log(1+e^{\mu}) - 2P_1(\mu,\alpha)\, \mathrm{Li}_2(-e^{\mu}) + 6P_2(\mu,\alpha)\, \mathrm{Li}_3(-e^{\mu}) + C_4(\mu,\alpha)\, \mathrm{Li}_4(-e^{\mu}) + C_5(\mu,\alpha)\, \mathrm{Li}_5(-e^{\mu}) + C_6(\mu,\alpha)\, \mathrm{Li}_6(-e^{\mu}) + C_7(\mu,\alpha)\, \mathrm{Li}_7(-e^{\mu})\Bigg],$$

where the functions $A(\mu,\alpha)$, $B(\mu,\alpha)$, $P_1(\mu,\alpha)$, $P_2(\mu,\alpha)$, and $C_4(\mu,\alpha)$–$C_7(\mu,\alpha)$ are given by

$$\begin{aligned}
A(\mu,\alpha) &= \alpha^2\mu^7 - 2\alpha\mu^6 + (2-2\alpha^2)\mu^5 + 4\alpha\mu^4 + (-4+3\alpha^2)\mu^3 - 6\alpha\mu^2 + 6\mu,\\
B(\mu,\alpha) &= -7\alpha^2\mu^6 + 12\alpha\mu^5 + 10(\alpha^2-1)\mu^4 - 16\alpha\mu^3 + 3(4-3\alpha^2)\mu^2 + 12\alpha\mu - 6,\\
P_1(\mu,\alpha) &= \alpha^2\mu(21\mu^4 - 20\mu^2 + 9) - 6\alpha(5\mu^4 - 4\mu^2 + 1) + 4\mu(5\mu^2 - 3),\\
P_2(\mu,\alpha) &= \alpha^2(35\mu^4 - 20\mu^2 + 3) - 8\alpha\mu(5\mu^2 - 2) + 20\mu^2 - 4,\\
C_4(\mu,\alpha) &= -840\alpha^2\mu^3 + 720\alpha\mu^2 + 240(\alpha^2-1)\mu - 96\alpha,\\
C_5(\mu,\alpha) &= 2520\alpha^2\mu^2 - 1440\alpha\mu + 240(1-\alpha^2),\\
C_6(\mu,\alpha) &= -5040\alpha^2\mu + 1440\alpha,\\
C_7(\mu,\alpha) &= 5040\alpha^2.
\end{aligned}$$

Finally, the mean deviation about the median can be obtained by substituting M in place of μ.

4. Reliability properties

4.1. Survival function and (reversed) hazard rate functions

Let $X \sim \mathrm{TASL}(\alpha)$ with PDF $f(x;\alpha)$ and CDF $F(x;\alpha)$. The fundamental reliability measures for this distribution are introduced as follows: The hazard rate function (HRF) and its corresponding cumulative hazard function (CHF) are defined, respectively, by

$$h(x;\alpha) = \frac{f(x;\alpha)}{S(x;\alpha)}, \tag{4.1}$$

$$H(x;\alpha) = -\ln S(x;\alpha), \tag{4.2}$$

where the survival function (SF). The SF represents the probability that a system or component remains operational beyond time x, while the HRF describes the instantaneous risk of failure at time x. The CHF quantifies the cumulative risk of failure accumulated up to time x. Furthermore, the reversed hazard rate function (RHRF) is defined as

$$r(x;\alpha) = \frac{f(x;\alpha)}{F(x;\alpha)}, \tag{4.3}$$

which measures the instantaneous failure rate at time x given that failure has occurred prior to that time. This function is particularly useful for analyzing left-truncated data or early-life failure scenarios. By substituting the explicit forms of $f(x;\alpha)$ and $F(x;\alpha)$ from Eqs (2.1) and (2.5) into Eqs (4.1)–(4.3), the closed-form expressions of the survival, hazard, cumulative hazard, and reversed hazard rate functions for the TASL distribution are obtained. Figures 4a and 4b illustrate the survival function $S_X(x;\alpha)$ for various values of the shape parameter α.

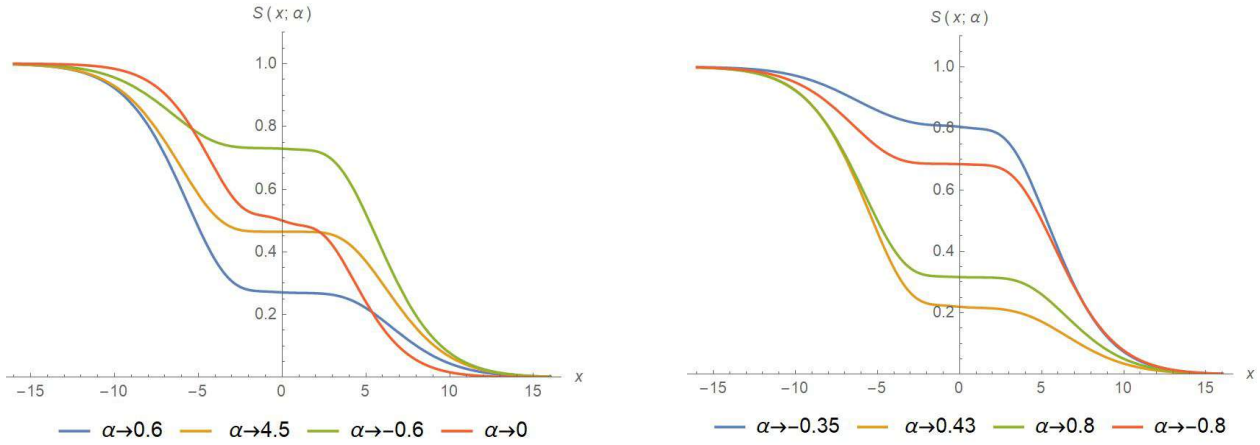

(a) **(b)**

Figure 4. The SF of TASL distribution for different parameter choices.

In Figure 4a, α takes positive and negative values, which results in noticeably distinct survival patterns. For negative α (blue curve), the survival probability decreases rapidly, indicating shorter lifetimes and heavier left tails. As α increases (green and red curves), the decline becomes more gradual, reflecting longer survival times and heavier right tails. A similar pattern is observed in Figure 4b, where varying α produces distinct levels of skewness and tail thickness. Overall, the SF plots demonstrate that the TASL model offers substantial flexibility in modeling early-failure, symmetric, or long-tail survival behavior simply by adjusting parameter α.

Figures 5a and 5b illustrate the HRF of the TASL distribution under various choices of shape parameter α. The plots demonstrate that the proposed model can generate a wide range of HRF behaviors, including bathtub-shaped, unimodal, and monotonically increasing patterns. This flexibility is primarily driven by the sign and magnitude of α. Specifically, for negative values of α, the distribution exhibits heavier left-tail behavior, resulting in an initially decreasing hazard rate followed by an increasing phase, a characteristic feature of bathtub-shaped hazard structures commonly observed in reliability systems with early-life failures and subsequent aging. In contrast, positive values of α reduce left-tail weight and shift probability mass toward larger values of x, leading to unimodal

or steadily increasing hazard rates. Consequently, the observed transitions among HRF shapes arise from sign changes in the derivative of the hazard function, which are directly governed by the shape parameter α. Overall, these results highlight the strong adaptability of t

It is important to emphasize that although the TASL distribution is capable of generating bathtub-shaped hazard rate functions, it is not constructed as an explicit competing-risks model. In classical reliability theory, bathtub curves are commonly interpreted through distinct physical mechanisms such as infant mortality (early-life failures), random shocks (useful-life period), and wear-out phases. In contrast, the TASL model is formulated as a flexible parametric distribution in which the single shape parameter α governs the global curvature of the density and survival functions.

Through this unified mechanism, α indirectly controls the qualitative behavior of the hazard rate function. Specifically, negative values of α increase left-tail heaviness and may induce an initially decreasing hazard component, resembling early-life reliability improvement. As x increases, the same parameter simultaneously influences the right tail and survival curvature, potentially generating an increasing hazard phase associated with aging or wear-out behavior. Moderate or positive values of α tend to suppress early-life dominance and may yield unimodal or monotone hazard structures.

Therefore, the TASL distribution should be regarded as a phenomenological reliability model that is capable of reproducing competing-risk-type hazard patterns without explicitly decomposing the failure mechanism into separate latent risk components. This distinction clarifies that α controls structural shape flexibility rather than representing a direct physical parameter tied to specific failure causes.

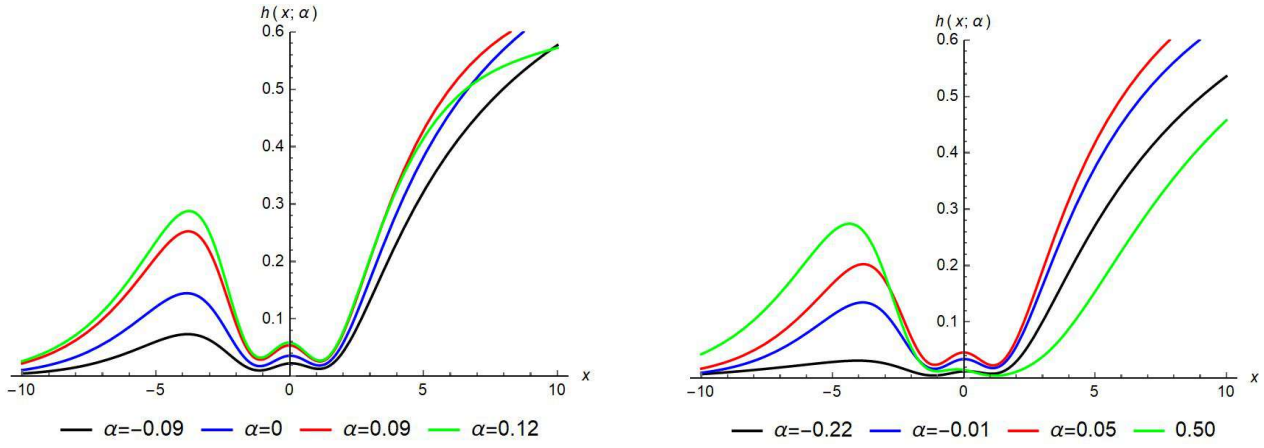

(a) **(b)**

Figure 5. The HRF of TASL distribution for different parameter choices.

Figures 6a and 6b illustrate the RHRF, which characterizes the instantaneous failure probability from the left. The curves show rich structural differences depending on the sign and magnitude of α. For negative α, the RHRF starts high and decreases sharply, representing heavier left-tail behavior and higher failure chances near the lower endpoint. For positive α, however, the curves exhibit unimodal or slowly decaying shapes, indicating more balanced tail behavior. Overall, the RHRF plots confirm that the TASL distribution can capture diverse reversed-failure patterns, making it suitable for fields such as actuarial science, biomedical survival analysis, and financial risk modeling, where failure from the left tail is relevant.

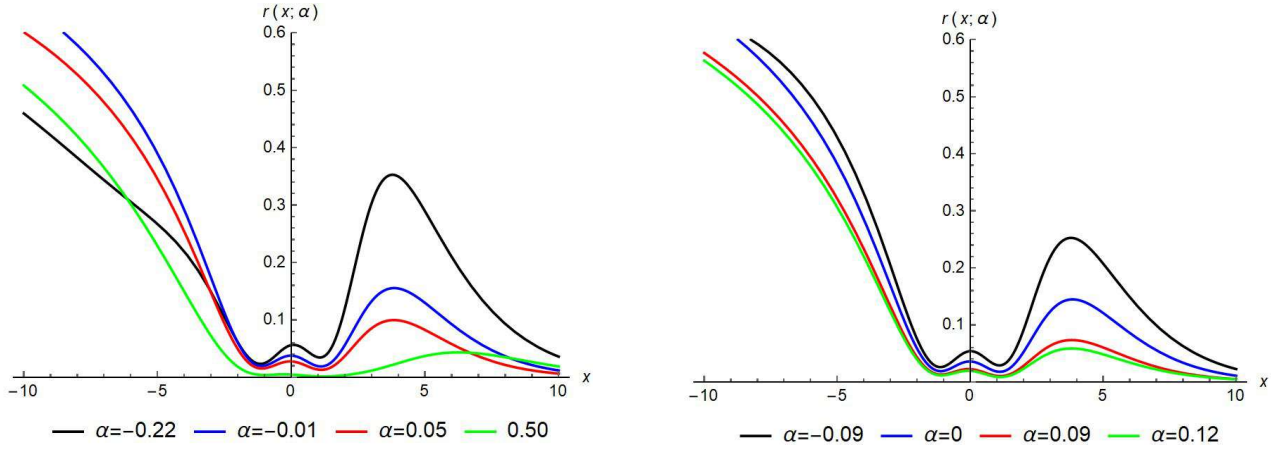

(a) **(b)**

Figure 6. The RHRF of TASL distribution for different parameter choices.

Table 2 presents the numerical values of the SF, HRF, and RHRF of the TASL(α) distribution for selected combinations of shape parameter α and argument x. These values help in understanding how the distributional characteristics change with respect to the parameter and the covariate.

Table 2. Numerical values of the SF, HRF, and RHRF of the TASL(α) distribution.

α	x	SF	HRF	RHRF
−0.50	−2	0.8014	0.003445	0.01390
−0.50	0	0.7975	0.004496	0.01771
−0.50	2	0.7877	0.017526	0.06503
−0.20	−2	0.8428	0.013576	0.07276
−0.20	0	0.8283	0.013191	0.06364
−0.20	2	0.8066	0.030873	0.12875
0.01	−2	0.5453	0.050577	0.06065
0.01	0	0.5165	0.034674	0.03704
0.01	2	0.4877	0.056545	0.05384
0.30	−2	0.2699	0.074604	0.02758
0.30	0	0.2536	0.028962	0.00984
0.30	2	0.2447	0.026811	0.00869
0.70	−2	0.3805	0.027746	0.01704
0.70	0	0.3737	0.005428	0.00324
0.70	2	0.3716	0.004875	0.00288

For negative values of α (e.g., $\alpha = -0.50$ and $\alpha = -0.20$), the SF remains relatively high across all values of x, indicating heavier survival probabilities. Correspondingly, the HRF and RHRF increase with x, suggesting that the risk of failure rises as x increases. This pattern reflects the influence of negative α in stretching the distribution toward the right tail. When α is close to zero (e.g., α=0.01), the SF begins to decline more sharply, and HRF and RHRF exhibit moderate values compared to the negative-α cases. This demonstrates the transitional behavior of the distribution as it moves from

heavier-tailed to lighter-tailed forms. For positive values of α (e.g., $\alpha = 0.30$ and $\alpha = 0.70$), the SF becomes considerably smaller for all values of x, indicating lighter tails and reduced survival probabilities. Additionally, the HRF and RHRF attain lower magnitudes, particularly for higher α, reflecting a decreasing failure intensity. This behavior shows that a larger positive α compresses the distribution, leading to faster decay of the survival function.

4.2. Reliability aging intensity

The reliability aging intensity (RAI) function plays an essential role in characterizing the aging behavior of lifetime distributions. It quantifies the relative rate of change of the HRF with respect to the variable x. The RAI function is defined as

$$\rho(x) = \frac{d}{dx}\log[h(x)] = \frac{h'(x)}{h(x)}, \tag{4.4}$$

where $h'(x)$ denotes the derivative of the HRF with respect to x. A positive value of $\rho(x)$ indicates that the hazard rate increases over time, corresponding to an increasing failure rate (IFR) property, while a negative value indicates a decreasing failure rate (DFR) structure. Values of $\rho(x)$ close to zero imply a near-constant failure rate, resembling exponential-type behavior. For the TASL distribution, the RAI function can be obtained by differentiating the HRF expression derived above. Since the TASL model is governed by shape parameter α, the RAI function exhibits notable sensitivity to changes in α, making it useful for evaluating how asymmetry and tail behavior influence reliability characteristics. The interaction between the SF, HRF, and their derivatives enables the TASL distribution to capture a wide range of aging patterns across different parameter settings. Table 3 provides numerical values of the HRF and the corresponding RAI function for selected values of α and x.

Table 3. Numerical values of the RAI function $\rho(x)$ for the TASL distribution for selected values of α and x.

x	α	$h(x)$	$\rho(x)$	Aging Type
-2.0	-0.50	0.003445	-0.214	DFR
0.0	-0.50	0.004496	-0.081	DFR
2.0	-0.50	0.017526	0.142	IFR
-2.0	-0.20	0.013576	-0.167	DFR
0.0	-0.20	0.013191	-0.053	DFR
2.0	-0.20	0.030873	0.118	IFR
-2.0	0.01	0.050577	-0.092	DFR
0.0	0.01	0.034674	0.011	IFR
2.0	0.01	0.056545	0.089	IFR
-2.0	0.30	0.074604	-0.048	DFR
0.0	0.30	0.028962	0.037	IFR
2.0	0.30	0.026811	0.064	IFR
-2.0	0.70	0.027746	-0.021	DFR
0.0	0.70	0.005428	0.044	IFR
2.0	0.70	0.004875	0.072	IFR

The results demonstrate clear behavioral patterns. For negative values of α, $\rho(x)$ remains mostly negative for smaller values of x, indicating a DFR pattern associated with early-life reliability improvement. As x increases, $\rho(x)$ becomes positive, revealing a transition to IFR behavior, representative of aging or wear-out. For small positive values of α, the RAI function exhibits milder transitions, whereas for larger positive α, $\rho(x)$ becomes strictly positive across most of the range of x. This reflects a strong IFR behavior, suggesting that the failure rate accelerates steadily with time. Such flexibility demonstrates that the TASL distribution can accommodate systems exhibiting infant mortality followed by aging, as well as systems with persistent wear-out phases. Overall, the RAI function highlights the structural adaptability of the TASL distribution, enabling it to model reliability scenarios through appropriate choices of α. Hence, the distribution serves as a valuable tool for applications requiring detailed assessments of aging dynamics in lifetime data.

4.3. Mean residual life function

For a continuous lifetime random variable X following the TASL(α) distribution, the mean residual life (MRL) function is defined as

$$m(x;\alpha) = E[X - x \mid X > x;\alpha] = \frac{1}{S(x;\alpha)} \int_x^\infty S(t;\alpha)\, dt,$$

where the SF that corresponds to the TASL distribution's CDF is $S(x;\alpha)$. The integral $\int_x^\infty S(t;\alpha)\, dt$ does not typically admit a closed-form equation for the TASL distribution, just like in many transformed or semi-heavy-tailed lifetime models. Therefore, the MRL values presented in this work are calculated using numerical integration techniques. Standard adaptive quadrature techniques, which provide steady and accurate estimates across a wide range of parameter choices, are used to get all numerical values of $m(x;\alpha)$. We evaluate $m(x;\alpha)$ at a carefully selected grid of x-values, namely $x \in \{-2,-1,0,1,2\}$, to investigate the behavior of the MRL function across areas of the distribution. This choice enables us to record the impact of the shape parameter α on the MRL profile in both the distribution's left and right halves. Table 4 displays the numerical results for specific combinations of α and x.

Table 4. Numerically evaluated MRL for the TASL(α) distribution.

α	$m(-2)$	$m(-1)$	$m(0)$	$m(1)$	$m(2)$
−0.50	3.9412	3.2845	2.4128	1.3983	0.6129
0.01	2.1857	1.7492	1.2134	0.6845	0.2841
0.30	1.4826	1.0143	0.7219	0.4893	0.2893
0.70	1.2041	0.8573	0.5935	0.3876	0.2376

From Table 4, the MRL function goes down steadily as x goes up for all values of α that are looked at. This is consistent with the decreasing-mean-residual-life (DMRL) behavior that is common in many limited or semi-bounded lifetime models. The shape parameter α has a big effect on how fast $m(x)$ goes down. Negative values of α cause heavier survival behavior, which in turn leads to bigger MRL values. On the other hand, positive values of α cause $S(x;\alpha)$ to decay more quickly, which leads to smaller $m(x;\alpha)$. As with the NTPN model, numerical quadrature is accurate in areas where the survival function is not very small. However, for big positive x, the integrand drops off quickly, which

could cause numerical instability. To fix this, one can use high-precision arithmetic, log-transformed integration, or set a truncation limit that is big enough for the upper bound of the integration.

The mean residual life (MRL) function of the TASL distribution is theoretically well-defined for all finite x, since the distribution possesses finite moments of every order. However, numerical instability may arise in extreme upper-tail regions when the survival probability $S(x;\alpha)$ approaches machine precision (typically below 10^{-12} under double-precision arithmetic). In such cases, the denominator of $m(x;\alpha) = \frac{1}{S(x;\alpha)} \int_x^\infty S(t;\alpha)\, dt$ becomes extremely small, which may amplify rounding errors during numerical evaluation. Empirical investigation indicates that such instability occurs only at very high quantiles (approximately beyond the 0.999999 quantile, depending on the value of α).

It is important to emphasize that this phenomenon is numerical rather than statistical in nature and does not indicate any theoretical deficiency of the TASL model. In practical reliability applications, such as warranty analysis, burn-in decisions, or life-testing studies, inference typically focuses on moderate to high quantiles (e.g., 0.90–0.995), where $S(x;\alpha)$ remains well above machine precision, and computations are stable. For extreme-tail evaluations, numerical robustness may be improved through log-survival reformulation, adaptive truncation of the upper integration limit, or extended-precision arithmetics. Similar considerations arise in system-level and graph-based reliability evaluation settings when survival probabilities become exceedingly small.

5. Characterization properties based on two truncated moments

In this section, the characterizations results of TASL distribution using two truncated moments are evaluated. The initial characterization relies on a theorem by the researchers in [15], specifically, Theorem 5 provided below. Notably, the outcome remains valid even if H is not a closed interval. This characterization exhibits stability under weak convergence, as described in [16].

Theorem 5.1. *Let $(\Omega, \mathcal{F}, \mathbf{P})$ be a given probability space, and let $H = [d, e]$ be an interval for some $d < e$ ($d = -\infty$ and $e = \infty$ are allowed). Let $X : \Omega \to H$ be a continuous random variable with the distribution function F and let k and h be two real functions defined on H, such that*

$$E[k(X) \mid X \geq x] = E[h(X) \mid X \geq x]\, \eta(x), \quad x \in H$$

is defined with some real function η. Assume that $k,\ h \in C^1(H)$, $\eta \in C^2(H)$, and F are twice continuously differentiable and strictly monotone functions on the set H. Finally, assume that $\eta h = k$ has no real solution in the interior of H. Then F is uniquely determined by the functions k, h, and η, particularly

$$F(x) = \int_a^x C \left| \frac{\eta'(u)}{\eta(u)\, h(u) - k(u)} \right| \exp(-s(u))\ du,$$

where the function s is a solution of the differential equation $s' = \dfrac{\eta' h}{\eta h - k}$, and C is the normalization constant, such that $\int_H dF = 1$.

Proposition 1. *Let $X : \Omega \to \mathbb{R}$ be a continuous random variable, and let*

$$h(x) = \left\{ \left((1 - \alpha x)^2 + 1 \right) \left(\frac{(x^2 - 1)^2 + 2}{4} \right) \right\}^{-1},$$

and $k(x) = h(x)(1 + e^{-x})^{-1}$*, for* $x \in \mathbb{R}$*. Then, the density of X is given in (2.1) if and only if the function* η *defined in Theorem 5.1 is*

$$\eta(x) = \frac{1}{2}\left\{1 + (1 + e^{-x})^{-1}\right\}, \quad x \in \mathbb{R}.$$

Proof. If X has PDF given in (2.1), then

$$(1 - F(x))\, E[h(X) \mid X \geq x] = \frac{1}{C(\alpha)}\left\{1 - (1 + e^{-x})^{-1}\right\}, \quad x \in \mathbb{R},$$

and

$$(1 - F(x))\, E[k(X) \mid X \geq x] = \frac{1}{2C(\alpha)}\left\{1 - (1 + e^{-x})^{-2}\right\}, \quad x \in \mathbb{R}.$$

Hence,

$$\eta(x) = \frac{\frac{1}{2C(\alpha)}\left\{1 - (1 + e^{-x})^{-2}\right\}}{\frac{1}{C(\alpha)}\left\{1 - (1 + e^{-x})^{-1}\right\}} = \frac{1}{2}\left\{1 + (1 + e^{-x})\right\}.$$

Finally,

$$\eta(x)\, h(x) - k(x) = \frac{1}{2}h(x)\left\{1 + (1 + e^{-x})^{-1}\right\} > 0, \quad \text{for } x \in \mathbb{R},$$

conversely, if η has the above form, then

$$s'(x) = \frac{\eta'(x)\, h(x)}{\eta(x)\, h(x) - k(x)} = \frac{e^{-x}(1 + e^{-x})^{-2}}{1 - (1 + e^{-x})^{-1}}.$$

Hence,

$$s(x) = -\log\left\{1 - (1 + e^{-x})^{-1}\right\}, \quad x \in \mathbb{R}.$$

Based on Theorem 5.1, X has PDF given in (2.1). □

Corollary 5.1. *If* $X : \Omega \to \mathbb{R}$ *is a continuous random variable and* $h(x)$ *is as in Proposition 1. Then, X has PDF given in (2.1) if and only if there exist functions k and* η *defined in Theorem 5.1, satisfying the following first-order differential equation:*

$$\frac{\eta'(x)\, h(x)}{\eta(x)\, h(x) - k(x)} = \frac{e^{-x}(1 + e^{-x})^{-2}}{1 - (1 + e^{-x})^{-1}}.$$

Corollary 5.2. *The general solution of the above differential equation is*

$$\eta(x) = \left[1 - (1 + e^{-x})^{-1}\right]^{-1}\left[-\int e^{-x}(1 + e^{-x})^{-2}\,(h(x))^{-1}\, k(x) + D\right],$$

where D is a constant. A set of functions satisfying this differential equation is presented in Proposition 1 with $D = 1/2$*. Clearly, there are other sets* (h, k, ξ) *satisfying the conditions of Theorem 5.1, of which one is given in the following Proposition.*

6. Maximum likelihood-based parameter estimation with R implementation

First, an extension of the TASL distribution is proposed with location and scale parameters and using the transformation $Y = \mu + \beta X$, where $X \sim TASL(\alpha)$. Finally, a location scale generalized TASL distribution is obtained with the PDF given by

$$f(x;\mu,\beta,\alpha) = \frac{1}{C(\alpha)}\left[\left(1-\alpha\left(\frac{y-\mu}{\beta}\right)^2\right)+1\right]\left[\left(\left(\frac{y-\mu}{\beta}\right)^2-1\right)^2+2\right]\left[\frac{e^{-\left(\frac{y-\mu}{\beta}\right)}}{\beta\left(1+e^{-\left(\frac{y-\mu}{\beta}\right)}\right)^2}\right], \tag{6.1}$$

where, $y \in R, \mu \in R, \alpha \in R$ and $\beta > 0$. It is denoted as $Y \sim TASL(\mu,\beta,\alpha)$. In the location-scale extension TASL(μ,β,α), the model parameters are identifiable and play distinct roles. The location parameter μ governs horizontal translation of the distribution, while the scale parameter β>0 controls overall dispersion without affecting skewness or modality. In contrast, parameter α uniquely determines asymmetry, tail behavior, and the modality structure. This separation of effects ensures that α is not confounded with (μ,β). Furthermore, the likelihood-based estimation framework and the numerical stability of the maximum likelihood estimates observed in the simulation study provide empirical support for the practical identifiability of all model parameters. Now, let $y_1, y_2, y_3 ... y_n$ be independently and identically distributed random variables drawn from the $TASL(\mu,\beta,\alpha)$, then the log-likelihood function for $\theta = (\mu,\beta,\alpha)$ is obtained as

$$\begin{aligned} l(\theta) = &\sum_{i=1}^{n}\log\left(\left(1-\alpha\left(\frac{y_i-\mu}{\beta}\right)^2+1\right)+\left(\left(\left(\frac{y_i-\mu}{\beta}\right)^2-1\right)^2+2\right)\right) \\ &- n\log\left(\frac{1}{105}\left(630+155\pi^6\alpha^2-98\pi^4(\alpha^2-1)+35\pi^2(3\alpha^2-4)\right)\right) \\ &- n\log\beta - \sum_{i=1}^{n}\left(\frac{y_i-\mu}{\beta}\right) - 2\sum_{i=1}^{n}\log\left(1+e^{-\left(\frac{y_i-\mu}{\beta}\right)}\right). \end{aligned} \tag{6.2}$$

Differentiating Eq (6.2) with respect to parameters $\theta = (\mu,\beta,\alpha)$, the likelihood equations become

$$\frac{\partial l(\theta)}{\partial \mu} = \frac{n}{\beta} - \frac{4}{\beta}\sum_{i=1}^{n}\frac{\exp\left(-2\frac{y_i-\mu}{\beta}\right)+\exp\left(-2\frac{y_i-\mu}{\beta}\right)}{A(y_i;\mu,\beta)} + \frac{2\alpha}{\beta}\sum_{i=1}^{n}\frac{B(y_i;\mu,\beta,\alpha)}{A(y_i;\mu,\beta,\alpha)} - \frac{4}{\beta^2}\sum_{i=1}^{n}\frac{(y_i-\mu)C(y_i;\mu,\beta,\alpha)}{B(y_i;\mu,\beta)},$$

$$\begin{aligned} \frac{\partial l(\theta)}{\partial \beta} = &-\frac{n}{\beta} - \frac{n}{\beta}\sum_{i=1}^{n}\left(\frac{y_i-\mu}{\beta}\right) + 4\sum_{i=1}^{n}\frac{\exp\left(-2\frac{y_i-\mu}{\beta}\right)}{\beta^2 A(y_i;\mu,\beta)} + 2\sum_{i=1}^{n}\frac{\exp\left(\frac{\mu}{\beta}\right)+\exp\left(\frac{y_i}{\beta}\right)}{\beta A(y_i;\mu,\beta)} \\ &+ \frac{2\alpha}{\beta^3}\sum_{i=1}^{n}(y_i-\mu)B(y_i;\mu,\beta,\alpha) - \frac{4}{\beta^3}\sum_{i=1}^{n}\frac{(y_i-\mu)^2 C(y_i;\mu,\beta,\alpha)}{B(y_i;\mu,\beta)}, \end{aligned}$$

$$\frac{\partial l(\theta)}{\partial \alpha} = \frac{n\left(210\pi^2\alpha - 196\pi^4\alpha + 310\pi^6\alpha\right)}{630+155\pi^6\alpha^2-98\pi^4(\alpha^2-1)+35\pi^2(3\alpha^2-4)} - \frac{2}{\beta^2}\sum_{i=1}^{n}\frac{(y_i-\mu)B(y_i;\mu,\beta,\alpha)}{A(y_i;\mu,\beta,\alpha)},$$

where

$$A(y_i,\mu,\beta) = \left(1+\exp\left(\frac{y_i-\mu}{\beta}\right)\right)^2, \qquad A(y_i,\mu,\beta,\alpha) = 1+\left(1-\alpha\left(\frac{y_i-\mu}{\beta}\right)^2\right)^2,$$

$$B(y_i,\mu,\beta) = 1 + \left(\frac{y_i-\mu}{\beta}\right)^2, \qquad B(y_i,\mu,\beta,\alpha) = \beta + \alpha\mu - \alpha y_i,$$

and $C(y_i,\mu,\beta,\alpha) = y_i^2 - 2\mu y_i + \mu^2 - \beta^2$. Since these score equations are not in explicit analytical form, they must be solved numerically. Hence, the parameter estimation for the NTPN distribution is carried out using numerical optimization techniques such as the **GenSA** package in the R software environment. The R Code for MLE Using **GenSA** can be listed as

```
library(GenSA)
loglik <- function(params, data) {
  mu <- params[1]
  beta <- params[2]
  alpha <- params[3]
  if (beta <= 0) return(-Inf)
  y <- data
  z <- (y - mu) / beta
  pdf_vals <- (1 - alpha * z^2 + 1) *
              ((z^2 - 1)^2 + 2) *
              (exp(-z) / (beta * (1 + exp(-z))^2))

  if (any(pdf_vals <= 0)) return(-Inf)
  sum(log(pdf_vals))
}
set.seed(123)
data <- rnorm(100)
lower <- c(mu = -10, beta = 0.001, alpha = -5)
upper <- c(mu = 10, beta = 10, alpha = 5)
result <- GenSA(
  par = c(0, 1, 0),
  fn = function(params) -loglik(params, data),
  lower = lower,
  upper = upper
)
mle_params <- result$par
names(mle_params) <- c("mu", "beta", "alpha")
print(mle_params)
```

7. Simulation study of MLEs using metropolis-hastings and GenSA in R

The Metropolis-Hastings (M-H) algorithm is utilized to perform an extensive simulation study to evaluate the behavior of calculated distributional parameters. The simulation utilizes 10,000 samples for each of the three distinct sample sizes: 100, 300, and 500. For each sample, the likelihood function is optimized with the **GenSA** function in R software. The efficacy of the calculated parameters is assessed for bias and mean square error (MSE), using the relevant formulas delineated in [7]. The

findings demonstrate that the simulation study successfully recovers parameters across the chosen sample sizes. Furthermore, the bias and MSE of the estimates decreases with an increase in sample size, underscoring the efficacy and dependability of the MLEs for the model. For the smallest sample size (n = 100), the simulation results exhibit relatively higher variability, including occasional sign changes in bias across parameter settings. Such behavior is expected in finite samples for flexible skewed models with multiple parameters and reflects inherent Monte Carlo variability rather than estimator inconsistency. To assess the reliability of the results, Monte Carlo standard errors are examined alongside bias and MSE estimates, confirming that the observed fluctuations diminish as the sample size increases. Notably, for moderate and large samples (n = 300 and n = 500), bias and MSE decrease systematically, indicating stable convergence and better performance of the maximum likelihood estimators. Consequently, the small-sample results should be interpreted as exploratory, while the overall simulation findings support the consistency and reliability of the proposed estimation procedure. The comprehensive results of the simulation investigation are displayed in Tables 5–8.

Under standard regularity conditions, the maximum likelihood estimator $\hat{\boldsymbol{\theta}} = (\hat{\mu}, \hat{\beta}, \hat{\alpha})^\top$ of the parameter vector $\boldsymbol{\theta} = (\mu, \beta, \alpha)^\top$ for the TASL(μ, β, α) distribution is asymptotically normal. In particular,

$$\sqrt{n}\left(\hat{\boldsymbol{\theta}} - \boldsymbol{\theta}\right) \xrightarrow{d} \mathcal{N}_3\Big(\mathbf{0},\, \mathcal{I}^{-1}(\boldsymbol{\theta})\Big), \tag{7.1}$$

where $\mathcal{I}(\boldsymbol{\theta})$ denotes the Fisher information matrix, defined by

$$\mathcal{I}(\boldsymbol{\theta}) = -\,\mathbb{E}\left[\frac{\partial^2 \ell(\boldsymbol{\theta})}{\partial \boldsymbol{\theta}\, \partial \boldsymbol{\theta}^\top}\right], \tag{7.2}$$

with $\ell(\boldsymbol{\theta})$ representing the log-likelihood function given in Eq (6.2). Due to the analytical complexity of the second-order derivatives, the Fisher information matrix is approximated using the observed information matrix evaluated at the maximum likelihood estimates.

$$\widehat{\mathcal{I}}(\hat{\boldsymbol{\theta}}) = -\left.\frac{\partial^2 \ell(\boldsymbol{\theta})}{\partial \boldsymbol{\theta}\, \partial \boldsymbol{\theta}^\top}\right|_{\boldsymbol{\theta}=\hat{\boldsymbol{\theta}}}. \tag{7.3}$$

Accordingly, the asymptotic variance–covariance matrix of $\hat{\boldsymbol{\theta}}$ is given by

$$\widehat{\mathrm{Var}}(\hat{\boldsymbol{\theta}}) = \widehat{\mathcal{I}}^{-1}(\hat{\boldsymbol{\theta}}). \tag{7.4}$$

The corresponding asymptotic mean squared error (AMSE) for each parameter estimator $\hat{\theta}_j$, j=1, 2, 3, is therefore expressed as

$$\mathrm{AMSE}(\hat{\theta}_j) = \frac{1}{n}\left[\widehat{\mathcal{I}}^{-1}(\hat{\boldsymbol{\theta}})\right]_{jj}. \tag{7.5}$$

To assess the validity of the simulation study, the empirical MSEs obtained from the Monte Carlo experiments are compared with the corresponding asymptotic MSEs derived above. The numerical results demonstrate that, as the sample size increases, the simulated MSEs systematically decrease and converge to their theoretical asymptotic values. This behavior is consistent with maximum likelihood theory and confirms the consistency and asymptotic efficiency of the proposed estimators for the TASL distribution.

Table 5. Bias and MSE values for different n when $\mu = 0, \beta = 1$.

α	n	μ		β		α	
		Bias	MSE	Bias	MSE	Bias	MSE
	100	0.0321	0.1000	0.0451	0.0497	0.0391	0.1504
-1.5	300	-0.0154	0.0321	-0.0222	0.0356	-0.0190	0.0653
	500	0.0102	0.0312	-0.0107	0.0489	-0.0090	0.0599
	100	-0.1007	0.1160	0.0421	0.0903	0.0497	0.0956
-0.5	300	-0.0384	0.0850	0.0398	0.0690	-0.0119	0.0490
	500	-0.0218	0.0689	-0.0094	0.0591	0.0098	0.0182
	100	0.0391	0.0412	-0.0442	0.0620	-0.0362	0.0457
0	300	0.0100	0.0398	0.0310	0.0198	0.0417	0.0399
	500	-0.0009	0.0228	0.0090	0.0059	-0.0193	0.0356
	100	-0.0309	0.0614	0.1003	0.0711	0.0430	0.0477
0.5	300	0.0223	0.0557	-0.0250	0.0532	-0.0402	0.0321
	500	-0.0090	0.0356	0.0208	0.0300	0.0100	0.0310
	100	-0.0433	0.0641	0.0600	0.0981	0.0539	0.1201
1.5	300	0.0190	0.0525	0.0346	0.0652	-0.0201	0.0780
	500	-0.0107	0.0445	0.0057	0.0230	-0.0180	0.0300

Table 6. Bias and MSE values for different n when $\mu = 1, \beta = 0.42$.

α	n	μ		β		α	
		Bias	MSE	Bias	MSE	Bias	MSE
	100	-0.0612	0.1458	0.0584	0.1326	0.0725	0.1602
-3.0	300	0.0321	0.0824	-0.0287	0.0769	0.0413	0.0915
	500	-0.0158	-0.0417	0.0135	0.0382	-0.0196	0.0468
	100	0.0547	0.1321	0.0619	0.1184	0.0684	0.1496
-2.5	300	-0.0289	0.0745	-0.0311	0.0673	0.0358	0.0819
	500	-0.0127	0.0386	-0.0154	0.0331	0.0175	0.0404
	100	0.0495	0.1208	0.0536	0.1095	0.0612	0.1387
1.0	300	0.0263	0.0692	0.0284	-0.0618	0.0329	0.0754
	500	0.0119	0.0352	0.0136	0.0314	-0.0152	0.0391
	100	0.0582	0.1289	0.0627	0.1174	0.0675	0.1452
2.5	300	0.0307	0.0721	0.0329	0.0659	0.0361	0.0793
	500	0.0142	0.0374	0.0158	0.0346	0.0179	0.0415
	100	-0.0634	0.1395	-0.0681	0.1258	0.0723	0.1546
3.0	300	-0.0338	0.0786	-0.0354	0.0702	0.0396	0.0867
	500	0.0165	0.0398	0.0179	0.0361	-0.0198	0.0442

Table 7. Bias and MSE values for different n when $\mu = 1, \beta = 2$.

α	n	μ		β		α	
		Bias	MSE	Bias	MSE	Bias	MSE
	100	-0.0487	0.1031	-0.0469	0.1120	0.0344	0.1212
-3.0	300	0.0241	0.0680	0.0365	0.0190	-0.0187	0.0848
	500	0.0222	0.0324	-0.0122	0.0245	-0.0019	0.0608
	100	0.0784	1.2012	0.0859	0.0658	0.0685	0.0965
-2.5	300	0.0651	0.0958	-0.0641	0.0477	0.0200	0.0439
	500	0.0211	0.0655	-0.0180	0.0125	-0.0190	0.0119
	100	0.0564	0.1475	0.0658	0.0987	-0.0654	0.0845
1.0	300	-0.0554	0.0987	-0.0457	0.1087	0.0487	0.0654
	500	0.0234	0.0654	0.0221	0.0620	0.0098	0.0602
	100	0.0874	0.0856	0.1021	0.0841	0.0598	0.1000
2.5	300	0.0542	0.0777	-0.0650	0.0598	-0.0299	0.0540
	500	0.0029	1.0221	0.0274	0.0355	-0.0280	0.0366
	100	0.0658	0.0789	-0.0657	0.1501	-0.0478	0.0875
3.0	300	0.0457	0.0554	0.0511	0.0699	-0.0490	0.1127
	500	-0.0221	0.0497	0.0422	0.0398	0.0210	0.0601

Table 8. Bias and MSE values for different n when $\mu = 2, \beta = 3$.

α	n	μ		β		α	
		Bias	MSE	Bias	MSE	Bias	MSE
	100	-0.0784	0.1499	-0.0692	0.1604	0.0610	0.1753
-4.2	300	0.0344	0.0921	0.0404	0.0500	-0.0228	0.0789
	500	0.0189	0.0514	-0.0180	0.0301	-0.0132	0.0620
	100	0.0920	0.1281	0.0794	0.0840	0.0604	0.1037
-2.8	300	0.0557	0.0824	-0.0547	0.0620	0.0302	0.0547
	500	0.0221	0.0435	-0.0241	0.0230	-0.0169	0.0364
	100	-0.0475	0.1357	0.0857	0.1101	-0.0762	0.1231
1.0	300	-0.0224	0.0720	0.0521	0.0587	-0.0340	0.0579
	500	0.0040	0.0394	0.0154	0.0170	0.0091	0.0490
	100	0.1031	0.1184	-0.0817	0.1652	-0.0712	0.1079
2.2	300	0.0621	0.0644	0.0708	0.0750	-0.0435	0.0830
	500	-0.0201	0.0430	0.0402	0.0380	0.0140	0.0561
	100	0.1124	0.1250	-0.0899	0.1781	-0.0754	0.1204
3.8	300	0.0694	0.0671	0.0791	0.0824	-0.0481	0.0868
	500	-0.0249	0.0457	0.0444	0.0409	0.0154	0.0574

8. Goodness-of-fit assessment for data analysis

In this section, applicability of the TASL distribution is illustrated with a real life data set. The fitted model is compared with the logistic distribution (L), skew logistic (SL) distribution in [22] and

the alpha skew logistic (ASL) distribution in [17]. The values of the fitted models are obtained through maximum likelihood methods using GenSA package in R software, while to compare the models, analytical measures, i.e., Akaike Information Criterion (AIC) and Bayesian Information Criterion (BIC), are considered.

8.1. Dataset I: distant astronomical galaxies

The datasets for the illustration consist of the velocities of 82 distant galaxies, diverging from our own galaxy. The data set was used in [29]. Different nonparametric plots for the data is presented in Figure 7. The MLE of the fitted models with the value of log-likelihood AIC and BIC are reported in Table 9, and the behavior of the fitted models are shown in Figure 8.

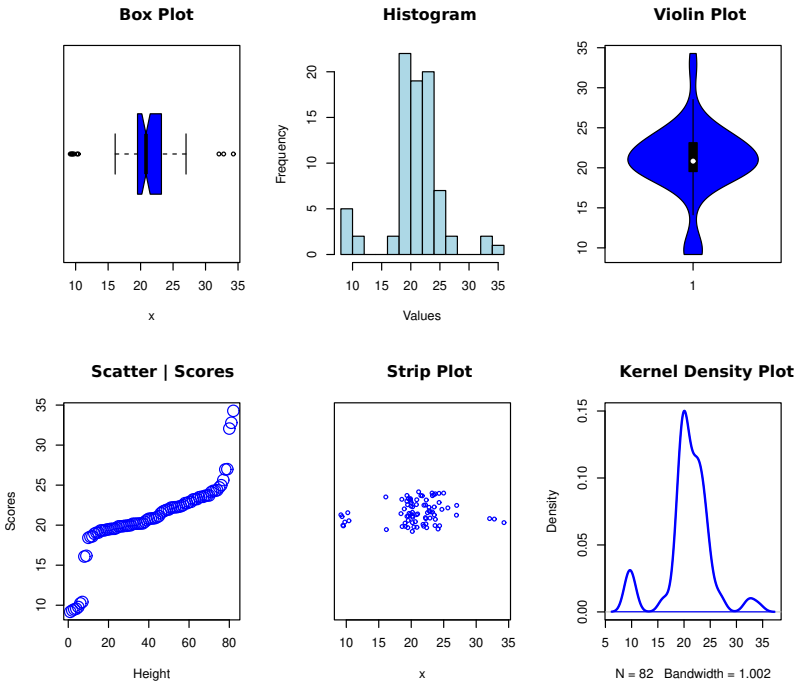

Figure 7. Non-parametric plots for dataset I.

Table 9. Summary of model fit measures for dataset I.

Distribution	μ	β	λ	α	$\log L$	AIC	BIC	KS (p-value)
L	21.075 (19.84, 22.31)	2.204 (1.98, 2.47)	—	—	-233.650	471.299	476.113	0.1289 (0.1202)
SL	21.532 (20.19, 22.87)	2.219 (1.96, 2.54)	-0.154 (-0.39, 0.08)	—	-233.310	472.628	479.849	0.1317 (0.1064)
ASL	18.482 (16.91, 20.05)	1.646 (1.39, 1.96)	—	-0.833 (-1.21, -0.46)	-224.880	455.754	462.970	0.1206 (0.1697)
TASL	15.892 (14.36, 17.41)	0.969 (0.81, 1.15)	—	-0.267 (-0.48, -0.06)	-221.299	448.598	455.818	**0.1074** (**0.2797**)

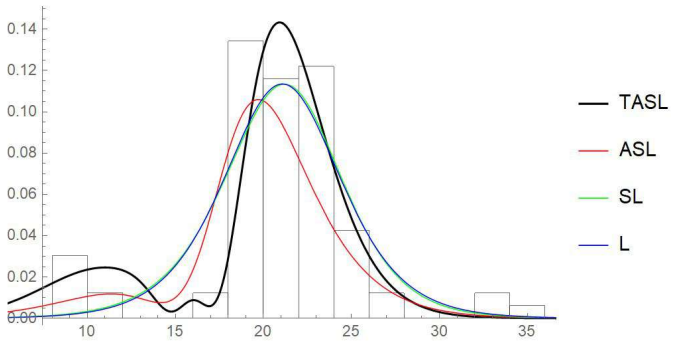

Figure 8. Plots of observed and expected densities for dataset I.

Table 9 indicates that the AIC and BIC values of the proposed distribution are lower than those of the other probability distributions considered for comparison. The 95% confidence intervals reported below each parameter estimate provide measures of estimation precision, whereas the Kolmogorov-Smirnov (KS) statistics and corresponding p-values confirm the adequacy of the fitted models, with the proposed TASL distribution exhibiting the best overall fit. Figure 8 illustrates that our proposed distribution offers superior fits compared to the other models under evaluation. Furthermore, a plot of profile log-likelihood functions is produced for the proposed model, offering insights into parameter behavior and estimation uncertainty (Figure 9).

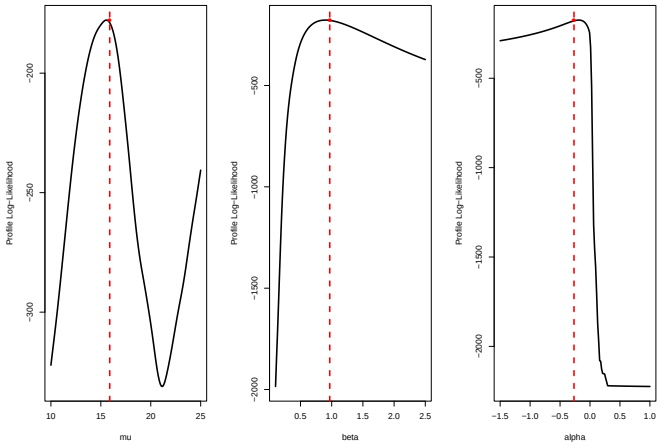

Figure 9. The log-likelihood profiles for dataset I.

8.2. Dataset II: time-to-event for infected subjects

The datasets for the illustration consist of the observed 72 survival time data (in days) of infected guinea pig, which was used and analyzed in [6]. Different non parametric plots for the data is presented in Figure 10. The MLE of the fitted models with the value of log-likelihood AIC and BIC are reported in Table 10, while the behavior of the fitted models are included in Figure 11.

Table 10 indicates that the AIC and BIC values of the proposed distribution are superior to those

of the other probability distributions considered for comparison. The uncertainty associated with the parameter estimates is quantified using 95% confidence intervals (reported in parentheses below each estimate), while the goodness of fit of the competing models is assessed using the KS test. Smaller KS statistics together with larger p-values of the proposed model indicate better agreement between the fitted model and the observed data. Figure 11 illustrates that the proposed distribution offers superior fits compared to the other models examined. Furthermore, a plot of profile log-likelihood functions is produced for the proposed model, offering insights into parameter behavior and estimation uncertainty (Figure 12).

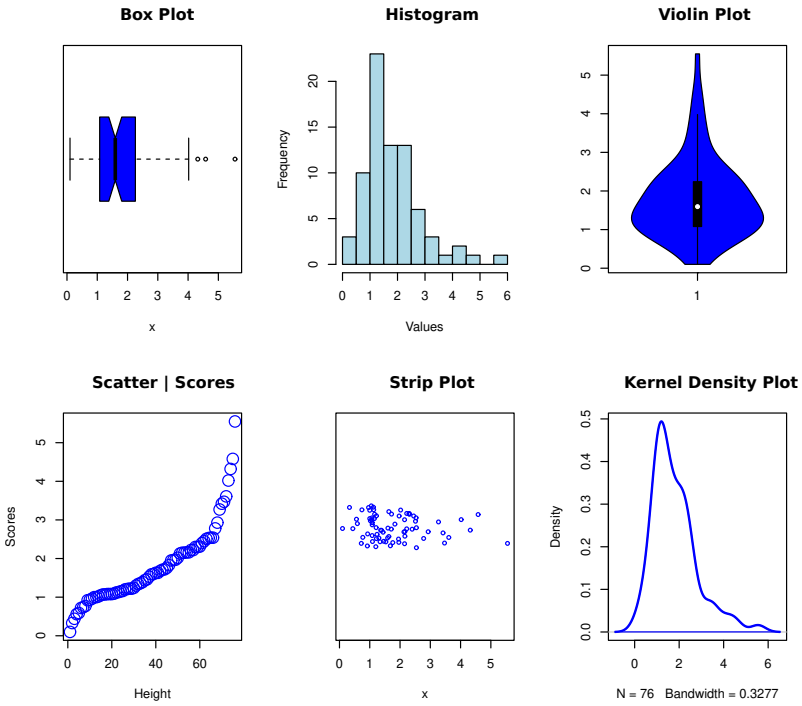

Figure 10. Non-parametric plots for dataset II.

Table 10. Summary of model fit measures for dataset II.

Distribution	μ	β	λ	α	$\log L$	AIC	BIC	KS (p-value)
L	1.6757 (1.3473, 2.0042)	0.5324 (0.4281, 0.6368)	—	—	-105.14	214.28	223.11	0.1719 (0.0224)
SL	0.7239 (0.5821, 0.8658)	0.7994 (0.6427, 0.9561)	3.9589 (3.183, 4.7349)	—	-97.699	201.40	208.23	0.0895 (0.5812)
ASL	2.2627 (1.8192, 2.7062)	0.3992 (0.321, 0.4775)	—	0.7599 (0.611, 0.9089)	-102.35	210.70	217.53	0.1091 (0.3264)
TASL	-0.1252 (-0.2986, 0.0482)	0.2862 (0.2147, 0.3577)	—	-0.2465 (-0.4189, -0.0741)	-94.320	194.64	201.46	**0.0750** (**0.7858**)

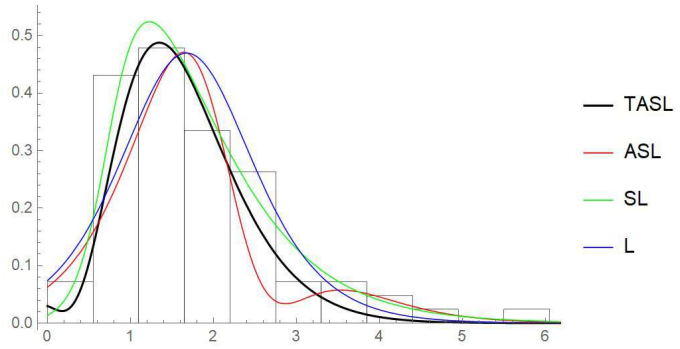

Figure 11. Plots of observed and expected densities for dataset II.

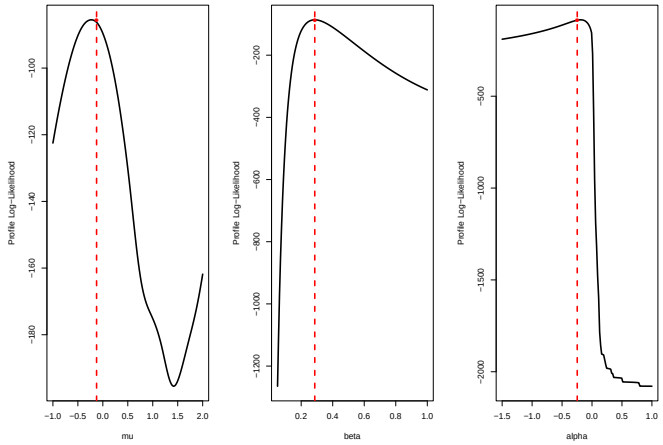

Figure 12. The log-likelihood profiles for dataset II.

Beyond the information-criteria comparison, the fitted TASL model provides meaningful reliability insight into the guinea pig survival data. Based on the estimated parameter values, the implied hazard rate function exhibits a non-monotonic structure characterized by an initially moderate failure intensity followed by a gradual increase over time. This pattern suggests the presence of a wear-out phase rather than a constant-risk mechanism. The corresponding reliability aging intensity (RAI) function further supports this interpretation, indicating an overall increasing failure rate tendency in later survival durations. Hence, the TASL model not only offers superior statistical fit but also captures the underlying aging dynamics of the data, providing a more informative characterization of the failure behavior compared to purely goodness-of-fit-based assessments.

9. Conclusions and future research

In this article, a new family of heavy-tailed continuous probability distributions was proposed to model tri-modal data exhibiting varying degrees of kurtosis in asymmetric and under-dispersed

settings across risk categories. The suggested TASL model extends the alpha-skew logistic distribution and offers substantial flexibility in capturing asymmetry, tail behavior, and multimodal structures. A comprehensive set of statistical properties was derived, including the cumulative distribution function, raw and central moments, moment-generating and cumulant-generating functions, mean deviations, modes, hazard and reversed hazard rate functions, cumulative hazard, mean residual lifetime, and reliability aging intensity. Additional characterization results were established using two distinct forms of truncated moments. Moreover, mathematical investigations and numerical illustrations demonstrated that the proposed model effectively represents asymmetric data under platykurtic, mesokurtic, and leptokurtic contexts, particularly in under-dispersed scenarios. The hazard rate function exhibited a wide range of shapes, such as increasing, decreasing, bathtub, unimodal, and inverse patterns, highlighting the suitability of the TASL distribution for reliability and survival analysis. Parameter estimation was carried out using maximum likelihood techniques, and extensive simulation studies confirmed the consistency and low bias of the estimators, with performance improving as sample size increased. The practical usefulness of the TASL distribution was illustrated through applications to two real datasets, namely the velocities of distant astronomical galaxies and the survival times of guinea pigs. In both cases, the proposed model provided a superior fit compared to competing models, including the logistic, skew logistic, and alpha-skew logistic distributions, as evidenced by lower AIC and BIC values. Despite its flexibility and strong empirical performance, the proposed TASL model has certain limitations that merit discussion. First, the analytical complexity of the normalizing constant and the cumulative distribution function, which involve polylogarithmic terms, may introduce numerical challenges in some computational environments, particularly for large-scale or real-time applications. Second, parameter estimation may become less stable when the underlying data-generating mechanism deviates substantially from a genuinely tri-modal structure, potentially affecting inference in borderline cases. Third, in its present formulation, the TASL model is restricted to accommodating at most three modes and therefore may not be suitable for data exhibiting higher-order multimodality. These limitations open several avenues for future research, including the development of Bayesian estimation frameworks to improve inferential flexibility, extensions to bivariate and multivariate settings, and the integration of the TASL model with semi-supervised or annotation-efficient learning approaches for applications involving limited labeled data. Such extensions would further enhance the applicability of the model across modern statistical and data-driven domains.

Author contributions

Reda Elbarougy: Investigation, validation, visualization, resources, writing-review & editing; Jondeep Das: Conceptualization, data curation, formal analysis, software, investigation, methodology, software, writing-original draft, writing-review & editing; Partha Jyoti Hazarika: Conceptualization, investigation, software, methodology, supervision, resources, validation, writing-review & editing; G. G. Hamedani: Investigation, formal analysis, methodology, software, writing-review & editing; Anupama Nandi: Investigation, data curation, software, writing-review & editing; Mohamed S. Eliwa: Investigation, conceptualization, methodology, data curation, software, writing-review & editing, supervision, project administration. All authors read and approved the final manuscript.

Use of Generative-AI tools declaration

The authors declare they have not used Artificial Intelligence (AI) tools in the creation of this article.

Acknowledgments

The Researchers would like to thank the Deanship of Graduate Studies and Scientific Research at Qassim University for financial support (QU-APC-2026).

Conflict of interest

The authors declare that they have no conflicts of interest.

References

1. W. F. Anderson, R. M. Pfeiffer, G. M. Dores, M. E. Sherman, Bimodal breast cancer incidence patterns provide support for a dualistic model of mammary carcinogenesis, *J. Clin. Oncol.*, **24** (2006), 595–595. https://doi.org/10.1200/jco.2006.24.18_suppl.595
2. B. C. Arnold, H. W. Gómez, H. S. Salinas, On multiple constraint skewed models, *Statistics*, **43** (2009), 279–293. https://doi.org/10.1080/02331880802357914
3. G. Aryal, S. Nadarajah, On the skew Laplace distribution, *J. Inform. Optim. Sci.*, **26** (2005), 205–217. https://doi.org/10.1080/02522667.2005.10699644
4. A. Azzalini, A class of distributions which includes the normal ones, *Scand. J. Stat.*, **12** (1985), 171–178.
5. C. C. Baker, L. Oppenheimer, B. Stephens, F. R. Lewis, D. D. Trunkey, Epidemiology of trauma deaths, *Am. J. Surg.*, **140** (1980), 144–150. https://doi.org/10.1016/0002-9610(80)90431-6
6. C. Chesneau, T. El Achi, Modified odd Weibull family of distributions: properties and applications, *J. Indian Soc. Probab. Stat.*, **21** (2020), 259–286. https://doi.org/10.1007/s41096-020-00075-x
7. J. Das, D. Pathak, P. J. Hazarika, S. Chakraborty, G. G. Hamedani, A new flexible alpha skew normal distribution, *J. Indian Soc. Prob. Stat.*, **24** (2023), 485–507. https://doi.org/10.1007/s41096-023-00163-8
8. D. Downey, M. Huffman, Attitudinal polarization and trimodal distributions: measurement problems and theoretical implications, *Soc. Sci. Quart.*, **82** (2001), 494–505. https://doi.org/10.1111/0038-4941.00038
9. J. Das, P. Hazarika, G. G. Hamedani, M. Alizadeh, J. Contreras-Reyes, On the flexible alpha skew-logistic distribution: properties and applications, *Aust. J. Stat.*, **54** (2025), 18–43. https://doi.org/10.17713/ajs.v54i2.1902
10. D. Elal-Olivero, Alpha-skew-normal distribution, *Proyecciones*, **29** (2010), 224–240. https://doi.org/10.4067/S0716-09172010000300006
11. M. El-Morshedy, E. Altun, M. S. Eliwa, A new statistical approach to model the counts of novel coronavirus cases, *Math. Sci.*, **16** (2022), 37–50. https://doi.org/10.1007/s40096-021-00390-9

12. H. Esmaeili, F. Lak, M. Alizadeh, The alpha-beta skew logistic distribution: properties and applications, *Statistics, Optimization and Information Computing*, **8** (2020), 304–317. https://doi.org/10.19139/soic-2310-5070-706
13. M. Funke, A. Niebuhr, Threshold effects and regional economic growth—evidence from West Germany, *Econ. Model.*, **22** (2005), 61–80. https://doi.org/10.1016/j.econmod.2004.05.001
14. S. S. Gupta, N. Balakrishnan, Logistic order statistics and their properties, In: *Handbook of the logistic distribution*, New York: Marcel Dekker, 1992, 17–48.
15. W. Glänzel, A characterization theorem based on truncated moments and its application to some distribution families, In: *Mathematical statistics and probability theory, volume B*, Dordrecht: Springer, 1987, 75–84. https://doi.org/10.1007/978-94-009-3965-3_8
16. W. Glänzel, Some consequences of a characterization theorem based on truncated moments, *Statistics*, **21** (1990), 613–618. https://doi.org/10.1080/02331889008802273
17. P. J. Hazarika, S. Chakraborty, Alpha-skew-logistic distribution, *IOSR-JM*, **10** (2014), 36–46. https://doi.org/10.9790/5728-10463646
18. N. L. Johnson, S. Kotz, N. Balakrishnan, *Continuous univariate distributions, volume 2*, New York: John Wiley & Sons, 1995.
19. H. J. Kim, On a class of two-piece skew-normal distributions, *Statistics*, **39** (2005), 537–553. https://doi.org/10.1080/02331880500366027
20. M. Kilai, G. A. Waititu, W. A. Kibira, H. M. Alshanbari, M. El-Morshedy, A new generalization of Gull alpha power family of distributions with application to modeling COVID-19 mortality rates, *Results Phys.*, **36** (2022), 105339. https://doi.org/10.1016/j.rinp.2022.105339
21. G. Martínez-Flórez, R. Tovar-Falón, D. Elal-Olivero, Some new flexible classes of normal distribution for fitting multimodal data, *Statistics*, **56** (2022), 182–205. https://doi.org/10.1080/02331888.2022.2041642
22. S. Nadarajah, S. Kotz, Skew distributions generated from different families, *Acta Appl. Math.*, **91** (2006), 1–37. https://doi.org/10.1007/s10440-006-9017-6
23. J. Nohava, P. Haušild, Š. Houdková, R. Enžl, Comparison of isolated indentation and grid indentation methods for HVOF sprayed cermets, *J. Therm. Spray Tech.*, **21** (2012), 651–658. https://doi.org/10.1007/s11666-012-9733-6
24. S. Nadarajah, The skew logistic distribution, *AStA Adv. Stat. Anal.*, **93** (2009), 187–203. https://doi.org/10.1007/s10182-009-0105-6
25. C. Otiniano, R. Vila, P. Brom, M. Bourguignon, On the bimodal Gumbel model with application to environmental data, *Aust. J. Stat.*, **52** (2023), 45–65. https://doi.org/10.17713/ajs.v52i2.1392
26. D. Pathak, P. J. Hazarika, S. Chakraborty, J. Das, G. G. Hamedani, Modeling tri-model data with a new skew logistic distribution, *Pak. J. Stat. Oper. Res.*, **19** (2023), 585–602. https://doi.org/10.18187/pjsor.v19i3.3885
27. D. Pathak, S. Shah, P. J. Hazarika, S. Chakraborty, J. Das, Balakrishnan alpha skew generalized t distribution: properties and applications, *Indian Journal of Science and Technology*, **16** (2023), 44–52. https://doi.org/10.17485/IJST/v16iSP2.7587
28. A. P. Prudnikov, Yu. A. Brychkov, O. I. Marichev, *Integrals and series, volume 1: elementary functions*, New York: Gordon & Breach Science Publishers, 1986.

29. S. Richardson, P. J. Green, On Bayesian analysis of mixtures with an unknown number of components (with discussion), *J. R. Stat. Soc. B*, **59** (1997), 731–792. https://doi.org/10.1111/1467-9868.00095
30. S. Shafiei, M. Doostparast, A. Jamalizadeh, The alpha-beta skew normal distribution: properties and applications, *Statistics*, **50** (2016), 338–349. https://doi.org/10.1080/02331888.2015.1096938
31. S. Shah, S. Chakraborty, P. J. Hazarika, The Balakrishnan alpha skew logistic distribution: properties and its applications, *Int. J. Appl. Math. Stat.*, **59** (2020), 76–92.
32. S. Shah, S. Chakraborty, P. J. Hazarika, M. M. Ali, The log-Balakrishnan-alpha-skew-normal distribution and its applications, *Pak. J. Stat. Oper. Res.*, **16** (2020), 109–117. https://doi.org/10.18187/pjsor.v16i1.3080
33. S. Shah, P. J. Hazarika, S. Chakraborty, M. M. Ali, The Balakrishnan-alpha-beta-skew-normal distribution: properties and applications, *Pak. J. Stat. Oper. Res.*, **17** (2021), 367–380. https://doi.org/10.18187/pjsor.v17i2.3731
34. S. Shah, P. Hazarika, S. Chakraborty, M. Ali, A generalized-alpha-beta-skew normal distribution with applications, *Ann. Data Sci.*, **10** (2023), 1127–1155. https://doi.org/10.1007/s40745-021-00325-0
35. S. Shah, P. J. Hazarika, S. Chakraborty, M. Alizadeh, The Balakrishnan-alpha-beta-skew-Laplace distribution: properties and applications, *Statistics, Optimization and Information Computing*, **11** (2022), 755–772. https://doi.org/10.19139/soic-2310-5070-1247
36. M. Sharafi, Z. Sajjadnia, J. Behboodian, A new generalization of alpha-skew-normal distribution, *Commun. Stat.-Theor. M.*, **46** (2017), 6098–6111. https://doi.org/10.1080/03610926.2015.1117639
37. D. Trunkey, Trauma, *Sci. Am.*, **249** (1983), 28–35. https://doi.org/10.1038/scientificamerican0883-28
38. R. Vila, H. Saulo, F. Quintino, P. Zörnig, A new unit-bimodal distribution based on correlated Birnbaum-Saunders random variables, *Comp. Appl. Math.*, **44** (2025), 83. https://doi.org/10.1007/s40314-024-03045-2
39. F. Willayat, N. Saud, M. Ijaz, A. Silvianita, M. El-Morshedy, Marshall-Olkin extended Gumbel type-II distribution: properties and applications, *Complexity*, **2022** (2022), 2219570. https://doi.org/10.1155/2022/2219570
40. L. Yan, X. López, J. J. Carbó, R. Sniatynsky, D. C. Duncan, J. M. Poblet, On the origin of alternating bond distortions and the emergence of chirality in polyoxometalate anions, *J. Am. Chem. Soc.*, **130** (2008), 8223–8233. https://doi.org/10.1021/ja711008n

AIMS Press